

Interstellar gas within ~ 10 pc of Sgr A*

Katia Ferrière¹

¹ IRAP, Université de Toulouse, CNRS, 14 avenue Edouard Belin, F-31400 Toulouse, France

Received ; accepted

ABSTRACT

Aims. We seek to obtain a coherent and realistic three-dimensional picture of the interstellar gas out to about 10 pc of the dynamical center of our Galaxy, which is supposed to be at Sgr A*.

Methods. We review the existing observational studies on the different gaseous components that have been identified near Sgr A*, and retain all the information relating to their spatial configuration and/or physical state. Based on the collected information, we propose a three-dimensional representation of the interstellar gas, which describes each component in terms of both its precise location and morphology and its thermodynamic properties.

Results. The interstellar gas near Sgr A* can be represented by five basic components, which are, by order of increasing size: (1) a central cavity with roughly equal amounts of warm ionized and atomic gases, (2) a ring of mainly molecular gas, (3) a supernova remnant filled with hot ionized gas, (4) a radio halo of warm ionized gas and relativistic particles, and (5) a belt of massive molecular clouds. While the halo gas fills $\approx 80\%$ of the studied volume, the molecular components enclose $\approx 98\%$ of the interstellar mass.

Key words. ISM: structure - Galaxy: center - Galaxy: nucleus - ISM: general - ISM: kinematics and dynamics - ISM: supernova remnants

1. Introduction

There is now compelling evidence, largely based on measured stellar orbits, that a massive black hole with mass $\approx 4 \times 10^6 M_\odot$ resides at the dynamical center of our Galaxy, which is traditionally identified with the compact nonthermal radio source Sagittarius A* (Sgr A*) (see Genzel et al. 2010, for a recent, comprehensive review). Sgr A* sits in the heart of a dense cluster of young, massive and luminous stars, which are concentrated within the central parsec and are distributed in two relatively thick disks that are highly inclined toward each other and rotate in opposite directions (Krabbe et al. 1991, 1995; Paumard et al. 2006). This central star cluster, which has a few bright condensations (notably, the IRS 16 complex at the very center), is the source of intense UV radiation and powerful stellar winds. Also present around Sgr A*, but extending much farther out, is a cluster of old and evolved, cool stars, with nearly isotropic distribution and slow, solid-body rotation (Blum et al. 2003; Trippe et al. 2008; Schödel et al. 2009). The old cluster dominates the stellar mass by far, with $\sim 10^6 M_\odot$ inside the central 1 pc (Schödel et al. 2009), as opposed to $\lesssim 1.5 \times 10^4 M_\odot$ in the young cluster (Paumard et al. 2006). Like in the rest of the Galaxy, all stars are immersed in an interstellar medium (ISM), which is essentially made of gas (in molecular, atomic and ionized forms) and dust.

The few-parsec region surrounding Sgr A* is of indisputable interest, not only in its own right, because it constitutes a unique, extremely complex and highly interacting Galactic environment, but also from a broader perspective, because it represents (by far) the nearest and, therefore, most easily accessible example of a galactic nucleus, and as such may be the key to understanding the energetic processes taking place in galactic nuclei in general. This is why the central few parsecs have long been the target of numerous observations over a wide range of frequencies. Recent

years have witnessed dramatic progress at both the low-energy (radio and infrared) and high-energy (X-ray and γ -ray) ends of the electromagnetic spectrum. Yet, despite the wealth of observational data that have now become available, achieving a clear and complete three-dimensional view of the innermost Galactic region remains a challenging task, due in large part to the difficulty in positioning the observed features along the line of sight.

In this context, we will try to unravel at best the intricate spatial distribution of the interstellar gas within ~ 10 pc of Sgr A*, and we will describe the emerging picture by way of a simplified three-dimensional gas representation, which we mean to be as realistic as possible. Let us specify from the outset that we will truly focus on the interstellar gas. Stars will only be alluded to for their direct impact on the interstellar gas, and interstellar magnetic fields will be tackled in a separate paper. Let us also emphasize that our purpose is not to provide a comprehensive overview of the interstellar gas in the region of interest. Instead, we will present what we feel are the most important and directly relevant observational studies. We will discuss their sometimes divergent results and extract the useful pieces of information that can serve as building blocks for our gas representation. We will then assemble all the pieces of information and try to reconstruct the overall puzzle. The existing observations will be presented in Section 2, while our gas representation will be the subject of Section 3.

Owing to the considerable uncertainties in the observational results and in their interpretations, which are reflected in the disparate conclusions reached by different authors, our gas representation will necessarily be approximate. However, we hope that it can be used as an observational input to theoretical studies that deal with Sgr A* and its surroundings. One such study that we have undertaken in parallel to the present work concerns the propagation and annihilation of positrons from Sgr A* (Jean et al., in preparation) – an important investigation in direct need of

Send offprint requests to: Katia Ferrière

a realistic and reasonably accurate description of the interstellar gas.

Unless stated otherwise, the observational maps presented here will be discussed in the equatorial coordinate system defined by right ascension, α , and declination, δ . In this system, east/west refers to the direction of increasing/decreasing α and north/south to the direction of increasing/decreasing δ (see Figure 1). We will also use the Galactic coordinate system defined by longitude, l , and latitude, b , where Galactic east/west refers to the direction of increasing/decreasing l and Galactic north/south to the direction of increasing/decreasing b . At the position of Sgr A*, the trace of the Galactic plane ($b = 0^\circ$) in the plane of the sky is at position angle $31^\circ 40'$ east of north (in J2000; Reid & Brunthaler 2004), so that there is a $58^\circ 60'$ angle between the (α, δ) and (l, b) systems.

Our gas representation will be described in terms of the Galactocentric cartesian coordinates, (x, y, z) , where x is the horizontal (i.e., parallel to the Galactic plane) coordinate along the line of sight to the Sun (positive toward the Sun), y the horizontal coordinate in the plane of the sky (positive toward Galactic east) and z the vertical (i.e., perpendicular to the Galactic plane) coordinate (positive toward Galactic north). For consistency with our previous papers on the Galactic center (GC) region, we will adopt $r_\odot = 8.5$ kpc for the Galactocentric radius of the Sun, such that angular separations of $1'$ and $1''$ translate into linear separations near Sgr A* of 2.5 pc and 0.04 pc, respectively.

The coordinates of Sgr A* in the three different systems are $(\alpha_{A^*}, \delta_{A^*}) = (17^h 45^m 40^s.04, -29^\circ 00' 28''.1)$ (in J2000; Reid & Brunthaler 2004), $(l_{A^*}, b_{A^*}) = (-0^\circ 03' 20''.5, -0^\circ 02' 46''.3)$ (as calculated using the (α, δ) coordinates of the origin of the (l, b) system given by Reid & Brunthaler 2004) and $(x_{A^*}, y_{A^*}, z_{A^*}) = 0$ (by construction). In the following, angular offsets with respect to Sgr A* will be denoted by $(\Delta\alpha, \Delta\delta)$ in the equatorial system and by $(\Delta l, \Delta b)$ in the Galactic system.

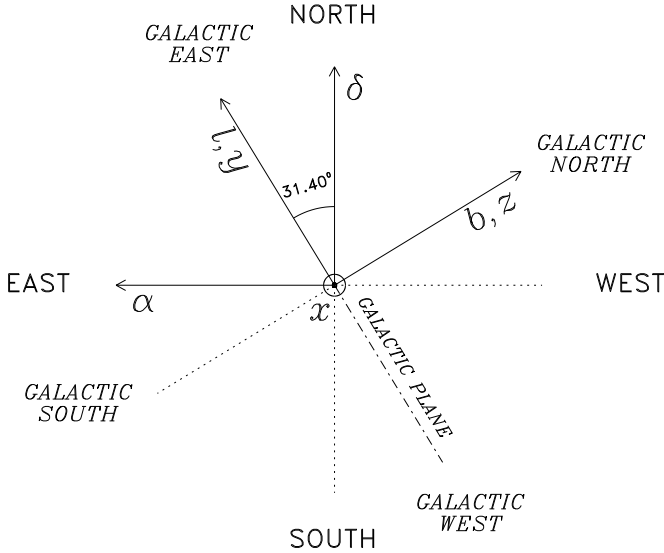


Fig. 1. Different coordinate systems used in this paper, shown in the plane of the sky: α (right ascension) and δ (declination) are the equatorial coordinates; l (longitude) and b (latitude) are the Galactic coordinates; and x (toward the Sun), y and z are the Galactocentric cartesian coordinates. See text for more details.

2. Observations of the interstellar gas

The interstellar gas in the immediate vicinity of Sgr A* has a complicated morphology (see, e.g., Morris & Serabyn 1996; Mezger et al. 1996, for early reviews). In brief, Sgr A* is embedded in a $\approx (2 - 3)$ pc sized cavity, the "Central Cavity", which was originally identified as a filamentary H II region named Sgr A West. This cavity has most likely been evacuated by stellar winds and photo-ionized by UV radiation from the central star cluster. Encircling the Central Cavity is an asymmetric torus of neutral (mainly molecular) gas and dust, usually referred to as the Circumnuclear Disk (CND) or, more appropriately, the Circumnuclear Ring (CNR). The CNR is generally interpreted as being part of an accretion disk around the central massive black hole, even though its pronounced asymmetry suggests that it is a transient feature. Both the Central Cavity and the CNR lie, in projection (onto the plane of the sky), inside a ≈ 10 pc scale non-thermal radio shell called Sgr A East and widely believed to be a supernova remnant (SNR). Sgr A East, in turn, is surrounded by a ≈ 20 pc diameter radio halo, which is probably composed of a mixture of warm ionized gas (thermal component) and relativistic particles (nonthermal component). Finally, a belt of massive molecular clouds around Sgr A East stretches over ≈ 30 pc along the Galactic plane; most prominent amongst these clouds are the well-known M-0.02-0.07 (or 50 km s^{-1}) and M-0.13-0.08 (or 20 km s^{-1}) giant molecular clouds (GMCs) located east and south, respectively, of Sgr A East. We now proceed to describe each of the above structural components in more detail.

2.1. The Central Cavity

The Sgr A West H II region appears in projection as a three-arm spiral, commonly known as the Minispiral and composed of the so-called Northern Arm, Eastern Arm and Western Arc as well as a short east-west Bar that connects the southern end of the Northern Arm and the western end of the Eastern Arm to the Western Arc (see Figure 2). It is now generally accepted that the Western Arc is the photo-ionized inner edge of the western part of the CNR (e.g., Lo & Claussen 1983; Serabyn & Lacy 1985; Güsten et al. 1987; Roberts & Goss 1993), while the Northern and Eastern Arms are the photo-ionized surfaces of tidally stretched streamers of material falling in toward the central massive black hole (e.g., Lo & Claussen 1983; Serabyn & Lacy 1985; Ekers et al. 1983; Davidson et al. 1992; Jackson et al. 1993). For completeness, we should mention that the Eastern Arm has also been suggested, by analogy with the Western Arc, to be the photo-ionized inner edge of the eastern part of the CNR (e.g., Aitken et al. 1998; Shukla et al. 2004). However, this suggestion appears to be incompatible with the finding that the Eastern Arm is nearly perpendicular to the CNR (Latvakoski et al. 1999) and to the Western Arc (Zhao et al. 2010).

Lo & Claussen (1983) presented a VLA 6 cm radio continuum map of the central 3 pc of the Galaxy, which clearly shows the spiral structure of Sgr A West. They estimated the total mass of ionized gas in the Minispiral at $\approx 60 M_\odot$, with $\approx 10 M_\odot$ in the Northern Arm, $\approx 10 M_\odot$ in the Eastern Arm, $\approx 35 M_\odot$ in the Western Arc (which they referred to as the south arm) and $\approx 5 M_\odot$ in the Bar (which they referred to as the west arm). They also estimated the electron density at $\approx 5 \times 10^4 \text{ cm}^{-3}$ in the brightest clumps and $\approx 10^3 \text{ cm}^{-3}$ in the lower-brightness features. Ekers et al. (1983), who mapped the Sgr A West region with the VLA at 2 cm, 6 cm and 20 cm, found that the Minispiral has projected dimensions $\approx 60'' \times 25''$ ($2.5 \text{ pc} \times 1.0 \text{ pc}$), with

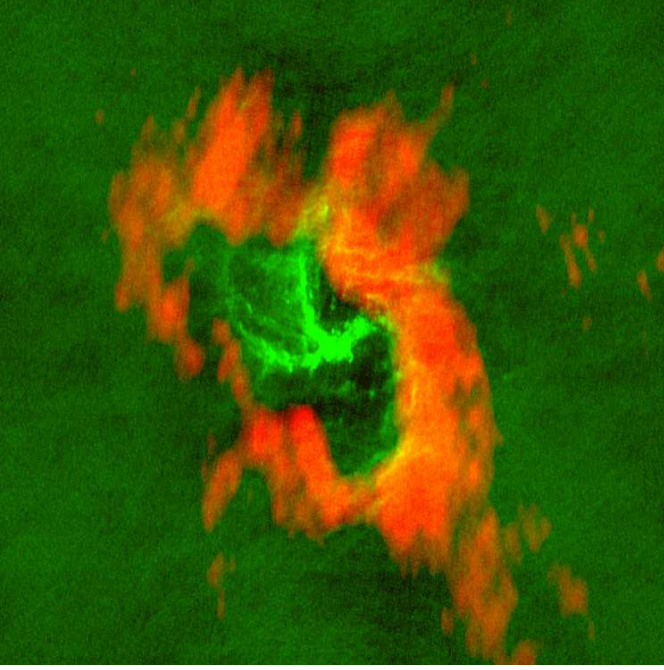


Fig. 2. Composite image showing (in green) the 3.6 cm radio continuum emission from warm ionized gas in the Sgr A West H II region, with the three-arm Minispiral emerging very clearly, and (in red) the 3.4 mm HCN $J = 1 \rightarrow 0$ line emission from the surrounding Circumnuclear Ring (CNR). The radio continuum data are from Yusef-Zadeh et al. (2008) and the HCN data from Wright et al. (2001). Figure credit: Farhad Yusef-Zadeh.

the long dimension along the Galactic plane, and for each of the three spiral arms, they derived an average emission measure $\approx 4 \times 10^6 \text{ pc cm}^{-6}$, an electron density $\approx 4 \times 10^3 \text{ cm}^{-3}$, and a total mass of ionized gas $\approx 15 M_{\odot}$ (assuming a filling factor of unity). They also detected diffuse emission from Sgr A West, over an area $\approx 75'' \times 40''$ ($3.1 \text{ pc} \times 1.6 \text{ pc}$), but they argued that this diffuse emission is mainly nonthermal and that most of the thermal emission from Sgr A West (at least at 6 cm) really comes from the Minispiral. Note that both Lo & Claussen (1983) and Ekers et al. (1983) assumed $r_{\odot} = 10 \text{ kpc}$, so that their estimated masses and densities need to be rescaled to our adopted value of $r_{\odot} = 8.5 \text{ kpc}$.¹

Similarly, by analyzing the VLA 2 cm radio continuum map of Brown & Liszt (1984), Beckert et al. (1996) found that the Minispiral is superimposed onto an extended Gaussian component with projected $FWHM$ dimensions $\approx 70'' \times 52''$ ($2.9 \text{ pc} \times 2.1 \text{ pc}$). However, they attributed the whole extended component to thermal (free-free) emission, which, for an electron temperature $\approx 6000 \text{ K}$, gave them a central emission measure $\approx 2 \times 10^6 \text{ pc cm}^{-6}$. Assuming, in addition, a line-of-sight depth $\approx 1 \text{ pc}$ and a filling factor of unity, they derived an electron density $\approx 1.4 \times 10^3 \text{ cm}^{-3}$ and a total H^+ mass $\approx 250 M_{\odot}$ for the extended component. For the Minispiral, they assumed a line-of-sight depth $\approx 0.1 \text{ pc}$ and obtained an electron density $\approx 10^4 \text{ cm}^{-3}$ and a total H^+ mass $\approx 9 M_{\odot}$. Hence, Beckert et al. (1996) came to the conclusion that, despite its spiral appearance, Sgr A West has most of its mass spread out throughout its volume. They also

remarked that their derived emission measure of the extended component is perfectly consistent with the emission measure $\approx 10^6 \text{ pc cm}^{-6}$ needed to explain the low-frequency turnover in the Sgr A* radio spectrum by foreground free-free absorption, if Sgr A* lies in the middle of Sgr A West and in front of the Minispiral.

Yusef-Zadeh et al. (1989) made higher-resolution VLA 2 cm and 6 cm radio continuum observations of Sgr A West, which brought out a number of fine-scale morphological details. For instance, they detected the stellar wind from the red supergiant IRS 7, located $\approx 0.25 \text{ pc}$ north of Sgr A*, and they suggested that this wind is photo-ionized externally by the UV radiation bathing the Central Cavity. They also observed the so-called Minicavity (first described by Morris & Yusef-Zadeh 1987) – a nearly circular, $\approx 0.08 \text{ pc}$ diameter hole in the distribution of ionized gas in the east-west Bar, centered $\approx 0.14 \text{ pc}$ south-west of Sgr A*. They naturally proposed that the Minicavity was swept out by a spherical stellar wind, although the most obvious stellar candidate, the IRS 16 complex, lies at the northeastern periphery of the Minicavity, not at its center. Other possible scenarios were later put forward. Roberts et al. (1996) suggested that the Minicavity is the ionized component of a compact molecular cloud moving along an orbit that passes very close to Sgr A*. Along different lines, Lutz et al. (1993) invoked a fast wind from one or more nearby sources which would blow into the Bar streamer and produce an expanding gas bubble there. Melia et al. (1996) proposed a more elaborate model, in which the central massive black hole gravitationally focuses the wind from IRS 16, partially accretes from it, and expels the rest in a collimated flow whose collision with the Bar streamer creates the Minicavity.

Sgr A West was also observed in various emission lines, starting with infrared lines such as the $12.8 \mu\text{m}$ [Ne II] fine-structure line (Lacy et al. 1979, 1980; Serabyn & Lacy 1985; Serabyn et al. 1988; Lacy et al. 1991), the $2.06 \mu\text{m}$ He I line (Hall et al. 1982; Geballe et al. 1991; Paumard et al. 2004), the $2.17 \mu\text{m}$ H I Br γ recombination line (Wright et al. 1989; Geballe et al. 1991; Herbst et al. 1993; Paumard et al. 2004), etc. The early infrared line emission images (see, e.g., Wright et al. 1989; Lacy et al. 1991) were found to closely resemble the 6 cm radio continuum map of Lo & Claussen (1983). Besides, Lacy et al. (1991) were able to reproduce the morphology and kinematics of much of the [Ne II]-emitting ionized gas with a one-armed linear spiral containing the Western Arc and the Northern Arm (but excluding the Eastern Arm and most of the Bar), along which the gas is in nearly circular Keplerian rotation about Sgr A*. The [Ne II] data of Lacy et al. (1991) were subsequently re-examined by Vollmer & Duschl (2000), who, in addition to circular rotation, allowed for turbulent motions plus slow radial accretion. They found that the Western Arc, the Northern Arm and part of the Bar are located in a single plane (the plane of the CNR), whereas the Eastern Arm is actually composed of two distinct pieces belonging to two different planes, one of which also encloses the rest of the Bar. Aside from the dense gas confined to the Minispiral, tenuous gas appears to fill the plane of the Western Arc + Northern Arm and possibly one of the planes of the Eastern Arm.

In parallel to infrared emission lines, which are plagued by interstellar dust extinction, radio emission lines have proven particularly valuable since the early work of van Gorkom et al. (1985) and Schwarz et al. (1989). Roberts & Goss (1993) carried out VLA observations of the 8.3 GHz (3.6 cm) H $_{92\alpha}$ recombination line to investigate the global kinematics and temperature distribution of Sgr A West. They found that the Western Arc,

¹ As a general rule, distances scale as r_{\odot} , surface densities as r_{\odot}^0 , volume densities as r_{\odot}^{-1} and masses as r_{\odot}^2 . However, when volume densities and masses are inferred from emission measures, they scale instead as $r_{\odot}^{-0.5}$ and $r_{\odot}^{2.5}$, respectively.

the Northern Arm and the extended bar (composed of the Eastern Arm, the Bar and its linear extension to the northwest) constitute three distinct kinematic entities. In contrast to the Western Arc, which appears to be in near circular rotation about Sgr A*, the Northern Arm and the extended bar do not appear to have significant circular motions. Roberts & Goss (1993) also derived the electron temperature in Sgr A West, by combining their H92 α line data with a 8.3 GHz continuum map and making the assumptions (all found to be satisfied in the case at hand) that the emitting gas is in local thermodynamic equilibrium (LTE), the continuum emission is thermal free-free, the continuum and recombination-line emissions are optically thin, and pressure broadening is negligible. Under these conditions, the line-to-continuum ratio implies an electron temperature ≈ 7000 K that is approximately uniform throughout Sgr A West.

Because radio recombination lines at centimeter wavelengths can be dominated by stimulated emission and affected by pressure broadening, Shukla et al. (2004) observed the Sgr A West region in the 92 GHz (3.3 mm) H41 α recombination line. At this higher frequency, the continuum and recombination-line emissions are believed to arise mostly in denser ionized gas. The morphology of the ionized gas in the 92 GHz continuum and H41 α line images is very similar to that in the 8.3 GHz continuum image of Roberts & Goss (1993). The Northern Arm appears to be ≈ 0.9 pc long, the Eastern Arm ≈ 0.4 pc, the Western Arc ≈ 1.5 pc, the Bar ≈ 1.1 pc, and the four spiral features are roughly 0.1 pc wide. Under the same assumptions as those made by Roberts & Goss (1993), Shukla et al. (2004) also derived a fairly uniform electron temperature ≈ 7000 K. At this temperature, the intensity of the continuum (supposedly thermal free-free) emission from the arms corresponds to an emission measure $\approx 2.5 \times 10^7$ pc cm $^{-6}$, which, if the line-of-sight thickness of the arms is comparable to their width (≈ 0.1 pc) and if the ionized gas in the arms is smoothly distributed (filling factor ≈ 1), implies an electron density $\approx 1.6 \times 10^4$ cm $^{-3}$ in the arms. The resulting H $^+$ masses are $\approx 2.8 M_\odot$ in the Northern Arm, $\approx 1.2 M_\odot$ in the Eastern Arm, $\approx 4.6 M_\odot$ in the Western Arc, $\approx 3.4 M_\odot$ in the Bar, and hence $\approx 12 M_\odot$ in the entire Minispiral.² Otherwise, the kinematics of the H41 α -emitting gas are essentially the same as those of the H92 α -emitting gas (see Roberts & Goss 1993).

A more complex picture of Sgr A West emerged from the work of Paumard et al. (2004), who observed the inner parts of the Minispiral in the 2.17 μ m H I Br γ and 2.06 μ m He I emission lines. A kinematic analysis of their data led them to identify nine coherent velocity components, comprising both extended, continuous flows and smaller, isolated patches. The most prominent component is the Northern Arm, which spreads well beyond the namesake filament seen in intensity maps, forming a wedge extending all the way over to the Eastern Arm. The latter is divided into three parts: two roughly parallel elongated features, named the Ribbon and the Eastern Bridge, and a smaller patchy feature at the western end, named the Tip. The Bar is straight and extends from the Ribbon to the Western Arc, which is only partly visible in the present, limited field of view. Then

² Strictly speaking, these estimates suppose that the Minispiral lies in the plane of the sky, which is almost certainly incorrect. In reality, if a section of an arm makes an angle θ with the plane of the sky, its estimated electron density and H $^+$ mass (at given emission measure) should be multiplied by $(\cos \theta)^{1/2}$ and $(\cos \theta)^{-1/2}$, respectively. However, a more important source of error is the uncertainty in the true width/thickness of the arms, which could possibly be as much as 2 times larger than quoted by Shukla et al. (2004). In this case, the electron density would be lower by a factor $2^{0.5} \approx 1.4$ and the H $^+$ masses larger by a factor $2^{1.5} \approx 2.8$.

come three small patchy features, named the Western Bridge, the Northern Arm Chunk and the Bar Overlay. Focusing on the Northern Arm, Paumard et al. (2004) showed that its kinematics could be mostly modeled with a system of Keplerian orbits about Sgr A*; these orbits are all close to the plane of the CNR, albeit not perfectly coplanar, such that they form a three-dimensional, saddle-shaped surface – like the inner surface of a torus. This kind of geometry would naturally come about if an infalling cloud was tidally stretched by the central massive black hole and had its inward-facing side photo-ionized by hot stars from, e.g., the IRS 16 complex. The warping of the flow surface would then give rise to orbit crowding in the plane of the sky, precisely along the bright filament seen in intensity maps. Finally, from the detection of two spots of extinction in the flux maps of the Northern Arm and the Bar, Paumard et al. (2004) concluded that, along the line of sight, the Bar lies behind the Northern Arm, which itself lies behind the Eastern Bridge.

Complementing the radial velocities extracted from infrared and radio spectral lines are the transverse velocities associated with proper motions. Yusef-Zadeh et al. (1998) measured proper motions of ionized gas in Sgr A West, based on VLA 2 cm radio continuum observations made at three epochs over a nine-year period. Their measurements revealed the existence of several features (notably, a head-tail structure dubbed the "bullet") with transverse velocities greater than the local escape velocities. The authors combined their measured transverse velocities with existing radial velocities from H92 α line data, whereby they found that most, and probably almost all, of the total velocities exceed the local escape velocities. From this, they concluded that ionized gas in the Northern Arm is probably on an unbound orbit – in agreement with Roberts et al. (1996), who attributed their measured H92 α radial velocities in the Minicavity to ionized gas being on a hyperbolic orbit about Sgr A*. Yusef-Zadeh et al.'s (1998) conclusion, which contradicts the widely accepted view that the Northern Arm is a tidally stretched streamer of infalling gas, could be explained if an energetic phenomenon, a few parsecs away from Sgr A*, pushed a gas cloud into the Galactic center.

Similarly, Mužić et al. (2007) performed the first proper motion measurements of infrared dust filaments in the Minispiral and showed that their shapes and velocities are *not* consistent with pure Keplerian rotation about Sgr A*. Instead, they could result from the dynamical interaction between a fast GC outflow and the Minispiral, where the GC outflow could either originate in the central cluster of young mass-losing stars, or emanate from the accreting black hole, possibly in the form of collimated jets (e.g., Yuan 2006), or even arise from a combination of both. Thus Mužić et al.'s (2007) filaments provide a new piece of circumstantial evidence for the existence of a GC outflow, adding to the Minicavity, which seems to be connected to Sgr A* by a chain of plasma blobs (Wardle & Yusef-Zadeh 1992; Melia et al. 1996); the bow-shock structure of the extended ionized envelope of IRS 7, with the apex facing toward Sgr A* or IRS 16 (Yusef-Zadeh & Melia 1992), and the associated cometary tail of ionized gas pointing directly away from Sgr A* (Yusef-Zadeh & Morris 1991); the similar bow-shock/cometary-tail morphology of IRS 3 (Viehmann et al. 2005); the observed waviness of the Northern Arm (Yusef-Zadeh & Wardle 1993); the narrow channel of low interstellar extinction running northeast-southwest through Sgr A*, with aligned cometary features (Schödel et al. 2007); etc.

The dynamics of the three ionized streams in Sgr A West were further studied by Zhao et al. (2009), who combined proper motion measurements for 71 compact H II features with radial

velocity measurements from archival H92 α line data. They were able to model the three ionized streams with three bundles of Keplerian elliptical orbits about Sgr A*, all three bundles being confined within the central 3 pc. They confirmed that the Western Arc stream is nearly circular, while the Northern and Eastern Arm streams have high eccentricities, and they suggested that the latter may collide in the Bar region, which they located mostly behind Sgr A*. They also found some support for Liszt's (2003) suggestion that the Eastern Arm and the Bar together form a single streamer. For future reference, the modeled orbital parameters of the three ionized streams (rescaled to $r_0 = 8.5$ kpc and adjusted to our line-of-sight vector pointing toward the Sun) are as follows: the Northern Arm has semimajor axis $a = 1.05$ pc, eccentricity $e = 0.83$, inclination (between the angular momentum vector and the line-of-sight vector) $i = 41^\circ$ and total length (calculated from the quoted range of true anomaly) $l = 2.7$ pc; the Eastern Arm (or Eastern Arm + Bar) has $a = 1.5$ pc, $e = 0.82$, $i = 58^\circ$ and $l = 3.5$ pc; and the Western Arc has $a = 1.2$ pc, $e = 0.20$, $i = 63^\circ$ and $l = 3.5$ pc.

Relying on the Keplerian model of Zhao et al. (2009), Zhao et al. (2010) drew a three-dimensional view of the three ionized streams, which clearly shows that the Northern Arm and Western Arc are nearly coplanar, that their mean orbital plane is nearly perpendicular to the orbital plane of the Eastern Arm, and that the Eastern Arm collides with the Northern Arm in the Bar region, just behind Sgr A*. More importantly, Zhao et al. (2010) presented new observations of the 232 GHz (1.3 mm) H30 α recombination line, which they interpreted together with previous H92 α line and 22 GHz continuum measurements in the framework of an isothermal, homogeneous, non-LTE H II model, to determine the physical parameters of the high-density ionized gas at selected positions (toward known infrared sources) along the Northern and Eastern Arms. They obtained electron kinetic temperatures in the range $\approx (5\,000 - 11\,000)$ K and electron densities in the range $\approx (10^4 - 10^5)$ cm $^{-3}$, with values up to $\approx 13\,000$ K and $\approx 2 \times 10^5$ cm $^{-3}$ in the Bar region. The higher electron temperatures and densities in the Bar region could result either from gas heating and compression by powerful winds from stellar clusters such as IRS 16 and IRS 13 or from the collision between the Northern and Eastern Arms.

In addition to warm ionized gas, the Central Cavity also contains substantial amounts of neutral atomic gas, detectable through atomic line emission (Genzel et al. 1985; Poglitsch et al. 1991; Jackson et al. 1993) and through dust thermal continuum emission (Davidson et al. 1992; Zylka et al. 1995; Telesco et al. 1996; Latvakoski et al. 1999). On the other hand, little molecular gas seems to be present, except possibly for a hot and dense molecular component detected in NH $_3$ (6, 6) emission very near Sgr A* (Herrnstein & Ho 2002). The general lack of molecular gas can be understood if any initially molecular cloud inside the Central Cavity has been largely photo-dissociated by the intense ambient UV radiation (Jackson et al. 1993; Latvakoski et al. 1999; Shukla et al. 2004).

The 63 μ m [O I] $^3P_1 \rightarrow ^3P_2$ line observations of Jackson et al. (1993) indicate that neutral atomic gas exhibits two prominent emission peaks on opposite sides of Sgr A*. The northern peak is part of a north-south, $\approx 1'$ (2.5 pc) long ridge of [O I] emission, which the authors interpreted as a streamer of neutral atomic gas falling through a gap in the CNR into the Central Cavity, between the Minispiral's Northern and Eastern Arms. The latter, they suggested, could simply be bright rims of ionized gas at the surface of this neutral "Northern Streamer" – a suggestion already made by Davidson et al. (1992), who

observed the Northern Streamer in dust far-infrared emission. Alternatively, only the Northern Arm would border the Northern Streamer, while the Eastern Arm would be an ionized rim at the surface of another infalling neutral streamer.³ The southern [O I] emission peak, for its part, is close to (but apparently slightly outside) the most prominent radio continuum emission peak in the Western Arc, which, we recall, is generally believed to be the ionized inner edge of the western portion of the CNR. By using their 63 μ m [O I] data toward the northern peak together with previous 146 μ m [O I] and 158 μ m [C II] data (from Genzel et al. 1985; Poglitsch et al. 1991) as input to model calculations of collisional excitation and radiative transport, Jackson et al. (1993) estimated that neutral (presumably atomic) gas inside the Central Cavity has a temperature $\approx (170 \pm 70)$ K, a true hydrogen density $\approx 3 \times 10^5$ cm $^{-3}$, a space-averaged hydrogen density $\approx 1.6 \times 10^3$ cm $^{-3}$ (beam-averaged hydrogen column density in a 55'' beam divided by an assumed line-of-sight pathlength of 1 pc; note, however, that the value reported in their Table 2 is too low by a factor of 2) and a total hydrogen mass (associated with the Northern and Eastern Arms) $\approx 300 M_\odot$.

Latvakoski et al. (1999) found that the three arms of the Minispiral seen in thermal radio continuum emission have counterparts in dust far-infrared continuum emission, which tend to lie $\approx 1'' - 3''$ farther from Sgr A*. This configuration, they explained, is consistent with the radio and far-infrared features being photo-ionized and photo-dissociated, respectively, by UV sources very close to Sgr A*. Latvakoski et al. (1999) also detected a far-infrared ring running along the inner edge of the CNR, with radial thickness $\approx 8'' - 11''$ (0.32 pc – 0.44 pc), and intersecting the far-infrared minispiral at its western arc.⁴ They naturally identified this far-infrared ring as the photo-dissociated inner layer of the CNR. The masses of (presumably photo-dissociated) hydrogen traced in the far-infrared are $\approx 110 M_\odot$ in the northern arm, $\approx 50 M_\odot$ in the eastern arm + bar, $\approx 660 M_\odot$ in the western arc, $\approx 1320 M_\odot$ in the full far-infrared ring and $\approx 16 M_\odot$ in the Central Cavity outside the minispiral. Note that the northern arm stretches $\approx 20''$ (0.8 pc) north beyond the CNR and that the 110 M_\odot mass refers only to its portion inside the CNR. The mean hydrogen densities near the southwest and northeast ends of the far-infrared ring, as obtained from the hydrogen column densities divided by a line-of-sight depth of 1 pc, are $\approx 1.6 \times 10^4$ cm $^{-3}$ and $\approx 4.0 \times 10^4$ cm $^{-3}$, respectively. Lastly, the dust temperature is found to be in the range $\approx (60 - 120)$ K. Latvakoski et al. (1999) proposed a simple, self-consistent dust model, adjusted to reproduce the far-infrared data as well as possible. In their model, the far-infrared ring (including the western arc) is nearly circular, with inner radius 1.58 pc, axial thickness 0.4 pc and inclination 65° to the plane of the sky. The northern arm and the eastern arm + bar are both on parabolic orbits about Sgr A*, 10° and 85° out of the plane of the CNR, respectively. The (poorly constrained) mean hydrogen densities are $\sim 1.2 \times 10^4$ cm $^{-3}$ in the far-infrared ring, $\sim 4 \times 10^4$ cm $^{-3}$ in the core of the northern arm, $\sim 2 \times 10^3$ cm $^{-3}$ in the core of the eastern arm + bar and ~ 25 cm $^{-3}$ in the Central Cavity outside the minispiral.

³ Clearly, the recent work of Zhao et al. (2010), which finds the Northern and Eastern Arms to be on nearly perpendicular orbits, makes the second scenario much more likely.

⁴ To avoid any possible ambiguity, we reserve upper case (Minispiral, Northern and Eastern Arms, Western Arc) for the original radio features, and use lower case (minispiral, northern and eastern arms, western arc) for their far-infrared counterparts.

The last gaseous component present inside the Central Cavity is a hot plasma, which was discovered with *Chandra* through its diffuse X-ray thermal emission (Baganoff et al. 2003). This hot X-ray emitting plasma extends across the central $\approx 20''$ (0.8 pc) of the Galaxy. A fit to its X-ray spectrum yields a temperature ≈ 1.3 keV (1.5×10^7 K) and an electron density $\approx (26 \text{ cm}^{-3}) \phi_h^{-1/2}$, where ϕ_h is the hot plasma filling factor. If the plasma is fully ionized and has twice the solar abundances, its total mass is $\approx (0.1 M_\odot) \phi_h^{1/2}$. Rockefeller et al. (2004) showed with three-dimensional numerical simulations that this hot plasma could be entirely explained as shocked gas produced in collisions between stellar winds.

2.2. The Circumnuclear Ring

The CNR has been observed in dust thermal continuum emission (e.g. Becklin et al. 1982; Mezger et al. 1989; Davidson et al. 1992; Dent et al. 1993; Telesco et al. 1996; Latvakoski et al. 1999) as well as in a wide variety of atomic and molecular tracers, including the 21-cm line of H I (Liszt et al. 1983), fine-structure lines of [O I] and [C II] (Genzel et al. 1985; Poglitsch et al. 1991), and various transitions of H₂ (Gatley et al. 1984, 1986; Depoy et al. 1989; Burton & Allen 1992; Yusef-Zadeh et al. 2001), CO (Liszt et al. 1985; Genzel et al. 1985; Harris et al. 1985; Serabyn et al. 1986; Güsten et al. 1987; Sutton et al. 1990; Bradford et al. 2005), OH (Genzel et al. 1985), CS (Serabyn et al. 1986, 1989; Montero-Castaño et al. 2009), HCN (Güsten et al. 1987; Marr et al. 1993; Jackson et al. 1993; Marshall et al. 1995; Wright et al. 2001; Christopher et al. 2005; Montero-Castaño et al. 2009), HCO⁺ (Marr et al. 1993; Wright et al. 2001; Shukla et al. 2004; Christopher et al. 2005), NH₃ (Coil & Ho 1999; McGary et al. 2001; Herrnstein & Ho 2005), etc. Collectively, these tracers lead to the picture of an asymmetric, extremely clumpy, torus-like CNR, with a sharp inner boundary at radius $\approx (1 - 1.5)$ pc and a more blurry, irregular outer boundary at radius $\approx (2.5 - 3)$ pc to the northeast and $\approx (4 - 7)$ pc to the southwest (see Figure 2). Besides, the CNR appears to be orbiting about Sgr A* and to have considerable internal motions.

Shortly after Becklin et al. (1982) discovered the CNR in dust far-infrared continuum emission, Genzel et al. (1985) observed it in several far-infrared emission lines, namely, in fine-structure lines of [O I] and [C II] and in rotational lines of CO and OH. Their observations revealed a disk or torus of neutral gas around the Central Cavity, with inner radius ≈ 1.4 pc, outer radius ≥ 4.2 pc (both rescaled to $r_\odot = 8.5$ kpc), inclination $\approx 69^\circ$ to the plane of the sky, and tilt $\approx 20^\circ$ to the Galactic plane. Atomic and molecular gases were found to be mixed throughout the disk/torus, with the fraction of atomic gas decreasing outward – as expected for a photo-dissociation region illuminated from inside. From the intensities of the [O I] and [C II] lines, Genzel et al. (1985) estimated the temperature of the atomic gas at ≈ 300 K and its true hydrogen density at $\approx 10^5 \text{ cm}^{-3}$. Furthermore, from existing dust far-infrared continuum emission data, they derived a space-averaged hydrogen density $\approx 7 \times 10^3 \text{ cm}^{-3}$ in the [O I] emission region (assuming a size $\approx (2 - 3)$ pc) and a total hydrogen mass $\approx 1.5 \times 10^4 M_\odot$ within a radius of 4.2 pc, while from existing CO $J = 1 \rightarrow 0$ line emission data, they derived a total hydrogen mass $\approx (1.5 - 3.7) \times 10^4 M_\odot$ in the purely molecular gas beyond 4.2 pc (all masses were rescaled to $r_\odot = 8.5$ kpc).

Subsequent CO and CS observations offered additional insight into the physical conditions of the CNR. Harris et al.

(1985) used their 0.37 mm CO $J = 7 \rightarrow 6$ line emission measurements in conjunction with previous measurements of two lower and two higher CO rotational lines to determine the H₂ density and gas temperature in CO-emitting regions. They obtained best-fit values $\approx 3 \times 10^4 \text{ cm}^{-3}$ and ≈ 300 K, respectively, and they restricted the range of acceptable density-temperature combinations to $(5 \times 10^5 \text{ cm}^{-3}, 150 \text{ K}) - (10^4 \text{ cm}^{-3}, 450 \text{ K})$. They also concluded that the CO-emitting gas is very clumpy, with a volume filling factor ~ 0.1 . Serabyn et al. (1986), who observed the CNR in 2.6 mm CO $J = 1 \rightarrow 0$ and 3.1 mm CS $J = 2 \rightarrow 1$ emission, inferred densities of a few 10^5 cm^{-3} for the CS-emitting gas, and derived a mass of molecular gas in the CNR $\geq 1.5 \times 10^4 M_\odot$ (rescaled to $r_\odot = 8.5$ kpc) from the measured CO flux. Sutton et al. (1990) combined their 0.87 mm CO $J = 3 \rightarrow 2$ observations with existing CO $J = 1 \rightarrow 0$ and $J = 7 \rightarrow 6$ data to find that the H₂ density and gas temperature in CO-emitting regions vary from $\approx 2 \times 10^5 \text{ cm}^{-3}$ and ≈ 200 K in the inner parts of the CNR to $\approx 2 \times 10^4 \text{ cm}^{-3}$ and ≈ 100 K in the outer parts. They also confirmed the clumpiness of the CO-emitting gas and estimated its volume filling factor at ~ 0.05 . The more recent CO $J = 7 \rightarrow 6$ observations of Bradford et al. (2005), which the authors analyzed together with published data on two lower and two higher CO rotational transitions, taking radiative transfer into account, yielded an H₂ density $\approx (5 - 7) \times 10^4 \text{ cm}^{-3}$ and a gas temperature $\approx (200 - 300)$ K.

Two other frequently used diagnostic molecules are HCN and HCO⁺. In the 3.4 mm HCN $J = 1 \rightarrow 0$ emission map of Güsten et al. (1987), the CNR emerges as an almost complete molecular ring centered $\approx 8''$ (0.32 pc) southeast of Sgr A*, which has projected major and minor mean diameters $\approx 95''$ and $50''$ (4.0 pc and 2.1 pc), respectively. The major axis has a position angle $\approx 30^\circ$ east of north, so that it is approximately aligned with the Galactic plane (see Figure 1). Moreover, if the ring is intrinsically circular, the aspect ratio $\approx 2 : 1$ implies an inclination angle $\approx 60^\circ$ out of the plane of the sky. The ring's inner and outer radii along the major axis are $\approx 30''$ and $65''$ (1.2 pc and 2.7 pc), respectively, but on the southwest side the HCN emission extends out to $\approx 100''$ (4.2 pc) – for comparison, Serabyn et al. (1986) derived an outer radius ≈ 7 pc for CO $J = 1 \rightarrow 0$ emission on the southwest side. The axial thickness of the whole HCN structure increases steadily with radius from ≈ 0.42 pc at 1.7 pc to ≈ 1.2 pc at 4.2 pc (rescaled to $r_\odot = 8.5$ kpc). Güsten et al.'s (1987) study also provides important kinematic information. The measured radial velocity peaks at $\approx 100 \text{ km s}^{-1}$, and its variation with position angle on the sky agrees reasonably well with that expected for rotation of a warped ring with rotation velocity $\approx 110 \text{ km s}^{-1}/135 \text{ km s}^{-1}$ and inclination angle $\approx 70^\circ/50^\circ$ in the southwest/northeast parts. In addition to this overall rotation, the gas exhibits strong turbulent motions with a velocity dispersion decreasing from an average of $\approx 55 \text{ km s}^{-1}$ near the inner edge to $\approx 37 \text{ km s}^{-1}$ near the southwest outer edge.

Jackson et al. (1993), who mapped a somewhat smaller area in the 1.1 mm HCN $J = 3 \rightarrow 2$ emission line, reached slightly different conclusions. They obtained a velocity-integrated HCN map similar to that of Güsten et al. (1987), but they interpreted the kinematic data in a different manner. Instead of invoking a single rotating ring that is warped, they appealed to four separate kinematic components, the most prominent of which is a rotating circular ring of peak radius $\approx (1.5 - 2)$ pc, inclination angle $\approx 65^\circ - 75^\circ$, position angle of the projected major axis $\approx 25^\circ$ east of north and rotation velocity $\approx 110 \text{ km s}^{-1}$. The other, weaker components are the so-called 50 km s^{-1} Streamer, 70 km s^{-1} Feature and -20 km s^{-1} Cloud. For the physical pa-

rameters of the molecular gas in the CNR, model calculations of HCN excitation and radiative transport yielded a temperature $\approx (50 - 200)$ K, a true H_2 density $\sim (10^6 - 10^8) \text{ cm}^{-3}$ and a space-averaged H_2 density $\sim (10^4 - 10^5) \text{ cm}^{-3}$ (assuming a line-of-sight pathlength of 1 pc through the CNR).

Wright et al. (2001) imaged the central 12 pc simultaneously in the 3.4 mm HCN and $\text{HCO}^+ J = 1 \rightarrow 0$ transitions, both of which are supposed to trace molecular gas with density $\sim (10^5 - 10^6) \text{ cm}^{-3}$. The two tracers present essentially the same velocity-integrated emission, and both indicate that the CNR is not a disk, but a well-defined ring peaked at radius $\approx 45''$ (1.9 pc) that extends radially from $\approx 20''$ to $60''$ (0.8 pc to 2.5 pc), with a southwest extension out to $\approx 120''$ (5 pc). Kinematically, the CNR is found to consist of two or three distinct streamers rotating around Sgr A* on separate orbits. The different inclinations of these orbits would be the reason for the warped-ring appearance of the CNR.

Christopher et al. (2005) performed additional HCN and $\text{HCO}^+ J = 1 \rightarrow 0$ observations with enhanced spatial resolution, which enabled them to study the internal structure of the CNR in greater detail. Their velocity-integrated maps are on the whole similar to those of Wright et al. (2001), and they, too, display a well-defined ring, although with slightly different dimensions. Here, the azimuthally-averaged HCN emission is found to peak at radii between $\approx 40''$ and $50''$ (1.7 pc and 2.1 pc), drop off steeply (over $\approx 10''$) on either side of the peak, and then decline much more gradually out past $\approx 150''$ (6.2 pc). Christopher et al. (2005) were able to resolve 26 dense molecular cores within the CNR, with typical sizes $\approx 7''$ (0.3 pc), and estimated their masses in two independent manners: virial masses were derived from the measured sizes and velocity widths, assuming the cores to be gravitationally bound, and optically-thick masses were derived from the measured sizes and HCN column densities, assuming an HCN-to- H_2 ratio of 10^{-9} (as opposed to 2×10^{-8} in Jackson et al. 1993) and multiplying by 1.36 to account for helium. Both masses were found to agree well, with median values $\approx 1.7 \times 10^4 M_\odot$ and $\approx 2.4 \times 10^4 M_\odot$, respectively, corresponding to mean H_2 densities inside the dense cores $\approx 4 \times 10^7 \text{ cm}^{-3}$ and $\approx 5 \times 10^7 \text{ cm}^{-3}$. From their derived core masses, Christopher et al. (2005) estimated the total mass of the CNR at $\approx 10^6 M_\odot$.

Remarking that the HCN and $\text{HCO}^+ J = 1 \rightarrow 0$ emission lines from the GC region are subject to self-absorption due to the intervening (cooler and more diffuse) molecular gas, Montero-Castaño et al. (2009) turned to the higher 0.85 mm HCN $J = 4 \rightarrow 3$ transition, which they observed toward the CNR, along with the 0.87 mm CS $J = 7 \rightarrow 6$ transition. They detected very clumpy emission from both tracers, with clumps arranged in a necklace-like fashion around the CNR. The southern part of the CNR has stronger emission and is found to be denser and warmer (from a comparison with the previously measured HCN $J = 1 \rightarrow 0$ line) than the northern part. Similarly, the inner edge of the CNR appears to be warmer than the outer parts – as expected if the CNR is heated by the intense UV radiation from the central star cluster. The clumps present wide ranges of physical characteristics, with sizes $\approx 3'' - 13''$ (0.12 pc – 0.5 pc), virial masses $\approx (0.4 - 60) \times 10^4 M_\odot$ and virial H_2 densities $\approx (2 - 40) \times 10^7 \text{ cm}^{-3}$. Summing the virial masses of all the HCN ($4 \rightarrow 3$) clumps listed by Montero-Castaño et al. (2009) gives a total CNR mass $\approx 1.3 \times 10^6 M_\odot$, comparable to the CNR mass estimated by Christopher et al. (2005).

The physical parameters of the CNR were very recently re-estimated by Oka et al. (2011), based on several millimeter and submillimeter molecular emission lines, including the

$J = 1 \rightarrow 0$ lines of CO, HCN, HCO^+ , N_2H^+ , HNC and SiO, the $J = 2 \rightarrow 1$ line of SiO and the $J = 3 \rightarrow 2$ line of CO. A one-zone large-velocity-gradient radiative-transfer analysis of a restricted set of lines (CO $J = 1 \rightarrow 0$, CO $J = 3 \rightarrow 2$ and HCN $J = 1 \rightarrow 0$), assuming $[\text{CO}]/[\text{H}_2] = 2.4 \times 10^{-5}$ and $[\text{HCN}]/[\text{H}_2] = 4.8 \times 10^{-8}$, concludes that the bulk of the CNR is made of molecular gas with kinetic temperature $\gtrsim 40$ K and H_2 density $\approx (5 \times 10^3 - 2 \times 10^4) \text{ cm}^{-3}$, the best-fit values being 63 K and $1.26 \times 10^4 \text{ cm}^{-3}$, respectively. Comparisons between the various line-intensity maps (most importantly, the CO and HCN $J = 1 \rightarrow 0$ maps) show that the innermost ring, at radius ≈ 2 pc, is both warmer and denser than the bulk of the CNR. The total H_2 mass of the CNR, estimated from the $^{13}\text{CO } J = 1 \rightarrow 0$ intensity map, is $\approx (2.3 - 5.2) \times 10^5 M_\odot$, which corresponds to the typical mass of GMCs in the GC region. Much larger is the virial mass of the CNR, estimated at $\approx 5.7 \times 10^6 M_\odot$. According to the authors, the important discrepancy between both masses strongly suggests that the CNR is not bound by self-gravity, but rather by the central mass. Finally, the CO $J = 3 \rightarrow 2$ data, interpreted with a simple kinematic model, point to a two-regime situation, where the bulk of the CNR is infalling at a speed $\approx 50 \text{ km s}^{-1}$, while the innermost ring at ≈ 2 pc is predominantly rotating.

Numerical simulations have greatly contributed to enhance our understanding of the CNR. For instance, the sticky-particle calculations of Sanders (1998) showed that the morphology and kinematics of the CNR could be explained by the tidal capture and disruption of a low angular-momentum cloud by the central massive black hole. The cloud would first be stretched into a long filament, which would wrap about the dynamical center and collide a few times with itself. Under the effect of viscous dissipation, the tidal debris would then settle into an asymmetric, precessing dispersion ring, which would persist for $\gtrsim 10^6$ yr. A similar scenario could apply to the Northern Arm (with its westward extension) inside the Central Cavity, although the original cloud would have to be smaller and on a lower angular-momentum orbit. It is interesting that, in the best-fitting simulation, the orbital plane of the extended Northern Arm lies at 10° of that of the CNR – which agrees well with the findings of Latvakoski et al. (1999), Paumard et al. (2004) and Zhao et al. (2010) (see Section 2.1).

2.3. The Sgr A East SNR

The nonthermal radio source Sgr A East clearly has a shell-like structure. The VLA 20 cm radio continuum map of Ekers et al. (1983) shows that this shell is elongated along the Galactic plane, with projected dimensions $\approx 3.6 \times 2.7$ (9.0 pc \times 6.7 pc), and that it is off-centered by ≈ 2.1 pc slightly north of east from Sgr A*. In projection, the western side of the Sgr A East shell overlaps with the Sgr A West H II region, and the Western Arc appears to smoothly merge into the shell. The shell-like morphology of Sgr A East, its measured size and its nonthermal (supposedly synchrotron) radio emission all converge to indicate that it is an SNR – as initially proposed by Jones (1974) and Ekers et al. (1975).

In the VLA 90 cm radio continuum image of Pedlar et al. (1989), the Sgr A East shell has projected dimensions $\approx 3.3 \times 2.1$ (8.2 pc \times 5.2 pc) and its major axis is at position angle $\approx 40^\circ$ east of north, i.e., roughly parallel to the Galactic plane (see Figure 1). On the western side of the radio shell, the spiral pattern of the Sgr A West H II region clearly stands out in absorption (free-free absorption by thermal gas) against the nonthermal emission from Sgr A East. This definitely places Sgr A West in front, or close to the near surface, of Sgr A East – as argued be-

fore by Yusef-Zadeh & Morris (1987), based on a comparison of 6 cm and 20 cm radio continuum maps. Yet not all of the 90 cm emission from Sgr A East is actually absorbed in this direction, which may indicate that Sgr A West lies within Sgr A East and close to its near surface (Yusef-Zadeh et al. 2000; see also Maeda et al. 2002). On the eastern side, the boundary of the radio shell is strikingly straight, which suggests that Sgr A East is colliding with the neighboring M–0.02–0.07 GMC.

Additional support for this suggestion comes from the 1.3 mm observations of Mezger et al. (1989), which reveal a dust ring surrounding the Sgr A East radio shell. This dust ring, with major inner diameter ≈ 10 pc along the Galactic plane, was also detected in OH and H₂CO absorption (Sandqvist 1974; Whiteoak et al. 1974) as well as in CO emission (see Mezger et al. 1996). Its eastern part coincides with a ridge of dense molecular gas in M–0.02–0.07 (see Section 2.5) and its southern part coincides with dense molecular gas belonging to M–0.13–0.08. Mezger et al. (1989) interpreted the observed ring as a shell of gas and dust surrounding the radio shell that is produced by the same supernova explosion. The reason why the gas-and-dust shell is particularly dense toward the east and south would be because in these directions the SNR has expanded into the M–0.02–0.07 and M–0.13–0.08 GMCs, respectively. Toward the west, the shell may have encountered Sgr A* and be captured (at least partially) by its gravitational pull, so as to form the present-day CNR. The authors also pointed out that the explosion seems to have dispersed most of the gas in front of Sgr A West, which could be explained if the explosion occurred inside a GMC, close to its near surface. The total hydrogen mass swept-up into the gas-and-dust shell was estimated at $\approx 6 \times 10^4 M_\odot$, which implies a mean preshock density $\sim 10^4 \text{ cm}^{-3}$ in the parent GMC.

The detection of 1720 MHz OH masers, without 1665 MHz and 1667 MHz counterparts, along the periphery of Sgr A East (Yusef-Zadeh et al. 1996, 1999a) revealed the presence of shocked molecular gas, thereby providing independent evidence that the expanding SNR is interacting with nearby molecular clouds. At the southeastern boundary of Sgr A East with the M–0.02–0.07 cloud, 1720 MHz OH masers were detected with radial velocities between 49 km s^{-1} and 66 km s^{-1} , i.e., close to the 50 km s^{-1} systemic velocity of the cloud, which reinforces the concept that the Sgr A East shock is propagating into M–0.02–0.07. 1720 MHz OH masers were also detected toward the CNR, with radial velocities of 134 km s^{-1} (at the intersection between the Northern Streamer and the CNR) and 43 km s^{-1} (along the outer western edge of the CNR). To confirm the presence of shocked molecular gas near the OH masers, Yusef-Zadeh et al. (2001) looked for $2.12 \mu\text{m}$ H₂ $v = 1 - 0 S(1)$ emission, and they found that all but one of the OH masers detected in the region are indeed accompanied by H₂ emission. In particular, the 43 km s^{-1} OH maser lies in projection along an H₂ filament, which extends over $\approx 1'$ along the western boundary of Sgr A East and peaks at velocities $\approx (50 - 75) \text{ km s}^{-1}$, close to the peak velocities of the western edge of the CNR. The location, morphology and kinematics of the H₂ filament and its likely association with a 1720 MHz OH maser strongly suggest that the filament was generated by the passage of the Sgr A East shock over the CNR (Yusef-Zadeh et al. 1999b). This, in turn, implies that Sgr A East must have engulfed part of the CNR.

Inside the cavity of the Sgr A East radio shell, Maeda et al. (2002) observed a hot X-ray emitting plasma with *Chandra*. They noted that the X-ray emission is concentrated within the central ≈ 2 pc of the radio shell. From the measured X-ray spectrum (continuum + K α emission lines from highly ionized

metals), they inferred a temperature $\approx 2.1 \text{ keV}$ ($2.4 \times 10^7 \text{ K}$) and an overabundance of heavy elements by a factor ≈ 4 with respect to solar levels, with an inward gradient in the abundance of iron relative to the other metals. Assuming a spherical volume of radius 1.6 pc, they derived an electron density $\approx (6 \text{ cm}^{-3}) \phi_h^{-1/2}$, a total gas mass $\approx (2 M_\odot) \phi_h^{1/2}$ and a total thermal energy $\approx (2 \times 10^{49} \text{ ergs}) \phi_h^{1/2}$, where again ϕ_h is the hot plasma filling factor. This estimated gas mass and thermal energy, together with the strong enrichment in heavy elements, lends credence to the long-standing idea that Sgr A East is an SNR. Moreover, the combination of shell-like nonthermal radio emission and centrally concentrated X-ray thermal emission classify this SNR as a mixed-morphology SNR.

Sakano et al. (2004) obtained a higher-quality X-ray spectrum of Sgr A East with *XMM-Newton*. Both their spectral fitting and their line-ratio analysis require at least two temperature components, at $\approx 1 \text{ keV}$ and $\approx 4 \text{ keV}$, respectively. The derived temperatures are somewhat lower in the core of the X-ray source ($\approx 0.9 \text{ keV}$ and $\approx 3 \text{ keV}$, respectively). The Fe abundance varies from ≈ 4 times solar in the core down to ≈ 0.5 solar in the outer region, whereas other metals (S, Ar, Ca) have more uniform abundances, all in the range $\approx (1 - 3)$ solar. If the core is approximated as a $28''$ (1.1 pc) radius sphere, and if the low- and high-temperature components within it are in thermal pressure balance and have a combined filling factor ϕ_h , their respective electron densities are $\approx (20 \text{ cm}^{-3}) \phi_h^{-1/2}$ and $\approx (6 \text{ cm}^{-3}) \phi_h^{-1/2}$. The corresponding total mass and thermal energy of hot plasma in the core are $\approx (1.4 M_\odot) \phi_h^{1/2}$ and $\approx (1.3 \times 10^{49} \text{ ergs}) \phi_h^{1/2}$, with 65% of the mass and 38% of the thermal energy in the low-temperature component. The distinct overabundance of Fe in the core (and not outside) suggests that the above estimates refer to stellar ejecta, which is consistent with a single supernova explosion. The rest of the X-ray emitting plasma is more likely shocked interstellar matter.

Much deeper *Chandra* observations than those of Maeda et al. (2002) enabled Park et al. (2005) to perform a spatially resolved spectral analysis of Sgr A East. They observed enhanced hard X-ray emission from a Fe-rich plasma over a $\approx 40''$ (1.7 pc) diameter region near the center of the SNR. They naturally identified this bright, Fe-rich plasma with stellar ejecta. Like Sakano et al. (2004), they fitted its hard X-ray spectrum with two temperatures (estimated here at $\approx 1 \text{ keV}$ and $\approx 5 \text{ keV}$) and they derived a high Fe abundance (≈ 6 times solar) compared to the S, Ar, Ca abundances ($\approx (0.7 - 1.8)$ solar). Park et al. (2005) also observed soft X-ray emission outside the hard X-ray core, in particular, in a plume-like feature extending toward the north of the SNR. They found that the emitting plasma in this feature could be characterized by a single temperature ($\approx 1.3 \text{ keV}$) and solar abundances, and they identified it with shocked interstellar matter. Park et al. (2005) also provided density estimates, both in the central Fe-rich core and in the northern plume-like feature. For the latter, they adopted a half-conical volume with a circular base of radius $\approx 25''$ and a height $\approx 50''$, and they obtained an electron density $\approx (7.4 \text{ cm}^{-3}) \phi_h^{-1/2}$. For the central core, they assumed a $\approx 40''$ diameter sphere with pure Fe²⁴⁺ ejecta, and they obtained electron densities $\approx (2.3 \text{ cm}^{-3}) \phi_h^{-1/2}$ and $\approx (0.5 \text{ cm}^{-3}) \phi_h^{-1/2}$ in the low- and high-temperature components, respectively, while they derived a total Fe ejecta mass $\approx (0.15 M_\odot) \phi_h^{1/2}$.

Finally, with *Suzaku*, Koyama et al. (2007) acquired a detailed X-ray spectrum of Sgr A East, which displays all the previously (firmly or tentatively) reported emission lines (K α lines

from He-like S, Ar, Ca, Fe; $K\alpha$ lines from H-like S, Ar, Fe) as well as a number of newly discovered emission lines ($K\alpha$ line from He-like Ni; $K\beta$ lines from He-like S, Ar, Fe; $K\gamma$ line from He-like Fe). The measured line ratios confirmed the necessary presence of at least two temperature components, while the complete spectral fitting required an additional hard tail. Altogether, the best-fit spectrum consists of two thin thermal components, with ≈ 1.2 keV and ≈ 6 keV, plus a power-law component, which could be caused by either a collection of point sources or non-thermal clumps and filaments. Koyama et al. (2007) found that, on average over the SNR, S, Ar, Ca have roughly solar abundances, while Fe is overabundant by a factor $\approx 2 - 3$, and they estimated the total mass of hot plasma at $\approx (27 M_{\odot}) \phi_h^{1/2}$.

2.4. The radio halo

The Sgr A East shell appears to be surrounded by an extended radio halo. In the VLA 20 cm radiograph of Yusef-Zadeh & Morris (1987), the radio halo has approximately the same shape (roughly elliptical), aspect ratio (~ 1.5), orientation (parallel to the Galactic plane) and center (northeast of Sgr A*) as Sgr A East, but it is about twice as large (~ 20 pc along its major axis). These properties suggest that Sgr A East and the radio halo are part of the same physical system. One possibility would be that the radio halo results from a leakage of cosmic-ray electrons accelerated in the Sgr A East SNR.

Pedlar et al. (1989) obtained more information on the nature and physical characteristics of the radio halo by combining VLA 90 cm, 20 cm and 6 cm continuum observations of the Sgr A complex. The radio halo is clearly visible in the 90 cm image, where it has a roughly triangular shape, with a total extent $\approx 7'$ (17.5 pc). The entire Sgr A East shell shows a low-frequency turnover in its nonthermal emission, which can be explained by free-free absorption by thermal ionized gas with an emission measure $\approx (1 - 2) \times 10^5$ pc cm $^{-6}$ (assuming an electron temperature ≈ 5000 K). Pedlar et al. (1989) suggested that the absorbing thermal gas belongs to the $7'$ radio halo. The radio halo itself has mainly nonthermal emission (at the considered wavelengths), and it, too, shows a low-frequency turnover explainable by free-free absorption. However, here, instead of residing in a separate foreground screen, the absorbing thermal gas is more probably mixed with the emitting nonthermal gas within the halo. In other words, the $7'$ radio halo is likely to comprise a mixture of thermal and nonthermal gases.

Pedlar et al. (1989) were able to reproduce the spectrum of the radio halo by adopting for the thermal gas an electron temperature ≈ 5000 K, an emission measure $\approx 2.7 \times 10^5$ pc cm $^{-6}$, and $FWHM$ dimensions $\approx 4' \times 4'$ (10 pc \times 10 pc), which, for a spherical distribution and a filling factor of unity, imply an electron density ≈ 165 cm $^{-3}$ and an H^+ mass $\approx 2100 M_{\odot}$ (rescaled to $r_{\odot} = 8.5$ kpc). Furthermore, since the thermal-gas free-free optical depths required to explain the low-frequency turnovers of the Sgr A East shell and of the radio halo are similar, Pedlar et al. (1989) suggested that the radio halo is mostly situated in front of Sgr A East. It should be noted, however, that within the uncertainties, the derived free-free optical depths are also consistent with only the near half of the radio halo lying in front of Sgr A East, so that Sgr A East could actually be deeply embedded within the radio halo, and even concentric with it.

The presence of warm ionized gas in the radio halo is confirmed by observations of radio recombination lines, which, in addition, provide useful kinematic information. VLA observations of the 1375 MHz (22 cm) H168 α recombination line

by Anantharamaiah et al. (1999) revealed an extended area of H168 α emission encompassing the entire Sgr A East shell and covering a broad range of radial velocities from ≈ -200 km s $^{-1}$ to $\approx +50$ km s $^{-1}$. The fact that the ionized gas observed in the H168 α line is detected neither in the lower-frequency H270 α line (sensitive to $n_e \lesssim 10$ cm $^{-3}$) nor in the higher-frequency H110 α and H92 α lines (sensitive to $n_e \gtrsim 1000$ cm $^{-3}$) constrains the electron density to lie in the range $n_e \sim (10 - 1000)$ cm $^{-3}$. The electron density can be additionally constrained by considering the H168 α data in conjunction with the radio spectrum of Sgr A East obtained by Pedlar et al. (1989) and by assuming that the H168 α emission arises in the same thermal ionized gas as the free-free absorption that is responsible for the low-frequency turnover of Sgr A East. In this manner, Anantharamaiah et al. (1999) found that a model with electron temperature $\approx 10^4$ K, emission measure $\approx 3.3 \times 10^5$ pc cm $^{-6}$ and electron density ≈ 100 cm $^{-3}$ gave a good fit to all the data combined. The H^+ mass predicted by this model is $\sim 8 \times 10^4 M_{\odot}$ (this is the value quoted by the authors, but we believe they meant an H^+ mass $\sim 8 \times 10^3 M_{\odot}$) over the $\sim 4' \times 4'$ projected area of Sgr A East.

Maeda et al. (2002) suggested that the halo of ionized gas roughly corresponds to the region of non-solid-body rotation around Sgr A*. This region would have a relatively homogeneous density, because differential rotation would have sheared and smoothed out the interstellar gas on a short ($\sim 10^5$ yr) timescale. Regarding the source of ionization, Maeda et al. (2002) ruled out collisional ionization, which would require too high a temperature. Instead, they argued in favor of photo-ionization by X rays, and they proposed that the ionizing X rays were emitted by Sgr A* $\sim (10^2 - 10^3)$ yr ago, during an episode of intense nuclear activity. This episode could have been triggered by the passage over Sgr A* of the gas-and-dust shell compressed by the Sgr A East forward shock. If this scenario is correct, Sgr A* should presently reside inside the Sgr A East cavity, consistent with Sgr A West itself residing inside Sgr A East (see Yusef-Zadeh et al. 2000).

Although the existence of a radio halo around Sgr A East leaves virtually no doubt, the presence of warm ionized gas within it is not universally accepted. For instance, the idea was called into question by Roy & Rao (2009), who measured the total flux densities of Sgr A East and the radio halo at five different frequencies ranging from 154 MHz (195 cm) to 1.4 GHz (21 cm). They observed similar low-frequency turnovers (at ~ 400 MHz) in the radio spectra of both sources, which they argued could be entirely attributed to free-free absorption in a common foreground screen, without requiring the presence of warm ionized gas inside the radio halo. From this, they concluded that the radio halo is in fact a purely nonthermal source.

2.5. The belt of molecular clouds

The geometry, kinematics and physical state of molecular clouds around the Sgr A complex have been investigated mainly through radio spectral lines of different molecules, including CO (Solomon et al. 1972), NH $_3$ (Güsten et al. 1981; Okumura et al. 1989, 1991; Coil & Ho 1999, 2000; McGary et al. 2001; Herrnstein & Ho 2002, 2005), CS (Serabyn et al. 1992; Tsuboi et al. 1999, 2006, 2009, see Figure 3), H $_2$ (Lee et al. 2003, 2008), CH $_3$ OH (Stankovic et al. 2007), HC $_3$ N (Sandqvist et al. 2008), SiO (Amo-Baladrón et al. 2009, 2011), etc., and also through dust submm continuum emission (e.g., Mezger et al. 1989; Zylka et al. 1990; Dent et al. 1993; Lis & Carlstrom 1994). The early CO emission map of Solomon et al. (1972) already revealed two massive molecu-

lar clouds peaking $\approx 3'$ east and $\approx 2.5'$ south of Sgr A* and having radial velocities in the range $\approx (45 - 65) \text{ km s}^{-1}$ and $\approx (15 - 35) \text{ km s}^{-1}$, respectively. Solomon et al. (1972) estimated their diameters at $\sim 6' - 20'$ and their hydrogen masses at $\geq 10^5 M_\odot$. Later, Güsten et al. (1981) carried out NH_3 observations of the region and derived a fairly uniform gas temperature $\approx (50 - 120) \text{ K}$ throughout the clouds. They also labeled the clouds M-0.02-0.07 and M-0.13-0.08, respectively, according to the Galactic coordinates of their NH_3 emission peaks. Today, these clouds are often referred to as the 50 km s^{-1} and 20 km s^{-1} clouds, respectively, although both denominations are not necessarily strictly equivalent. For instance, some authors include into the 50 km s^{-1} cloud not only M-0.02-0.07, but also several molecular knots on its positive-longitude side.

Zylka et al. (1990) made a first important attempt to obtain a coherent three-dimensional picture of molecular clouds in the central $\sim 50 \text{ pc}$. To locate gas along the line of sight, they compared their 1.3 mm dust emission map to a $2.2 \mu\text{m}$ intensity map showing dust absorption against the emission from the central star cluster, and to determine the gas kinematics, they resorted to isotopic CO and CS spectroscopy. In this manner, they found that M-0.02-0.07 is actually composed of two separate clouds, which they designated the Sgr A East Core and the Curved Streamer. These two clouds, together with M-0.13-0.08, were found to have the following properties:

- M-0.13-0.08, situated south of Sgr A East, has projected dimensions $\approx 15 \text{ pc} \times 7.5 \text{ pc}$ (with major axis roughly parallel to the Galactic plane), hydrogen mass $\approx 3 \times 10^5 M_\odot$ and radial velocities increasing with Galactic longitude from $\approx 5 \text{ km s}^{-1}$ to $\approx 25 \text{ km s}^{-1}$. Along the line of sight, the cloud lies in front of Sgr A* (as already pointed out by Güsten & Downes 1980, based on H_2CO absorption), at a possible distance $\sim 50 \text{ pc}$.
- The Sgr A East Core, which surrounds the Sgr A East radio shell, is $\geq 15 \text{ pc}$ in size and contains $\geq 2 \times 10^5 M_\odot$ of hydrogen. While it exhibits very high (positive and negative) turbulent velocities, its bulk radial velocity typically ranges from $\approx 40 \text{ km s}^{-1}$ to $\approx 70 \text{ km s}^{-1}$. Along the line of sight, it lies immediately behind Sgr A*. Clearly, the Sgr A East Core contains the gas-and-dust shell observed by Mezger et al. (1989), and it can be identified with the GMC inside which the supernova explosion that created Sgr A East took place.⁵
- The Curved Streamer, which stretches east of Sgr A East from the northern end of M-0.13-0.08 up to the eastern part of the Sgr A East Core, is $\approx 7.5 \text{ pc}$ wide in b , contains $\approx (1 - 1.5) \times 10^5 M_\odot$ of hydrogen and has radial velocities increasing steeply with Galactic longitude from $\approx 25 \text{ km s}^{-1}$ to $\approx 65 \text{ km s}^{-1}$. It lies in front of Sgr A*, with its southern end connecting with M-0.13-0.08 and its northern end pointing deeper inward, though probably not deep enough to connect with the Sgr A East Core.

The above GMCs are embedded in a clumpy and highly turbulent molecular intercloud medium, with estimated hydrogen mass $\sim 10^6 M_\odot$ (in the inner $\sim 50 \text{ pc}$), average density $\sim 10^2 \text{ cm}^{-3}$ and radial velocities in the range ≈ -40 to $+90 \text{ km s}^{-1}$.

Serabyn et al. (1992), who mapped M-0.02-0.07 in the CS $J = 5 \rightarrow 4$ and $J = 7 \rightarrow 6$ transitions (at 245 GHz and 343 GHz, respectively), also came to the conclusion that this cloud consists of two components: a dense molecular core peak-

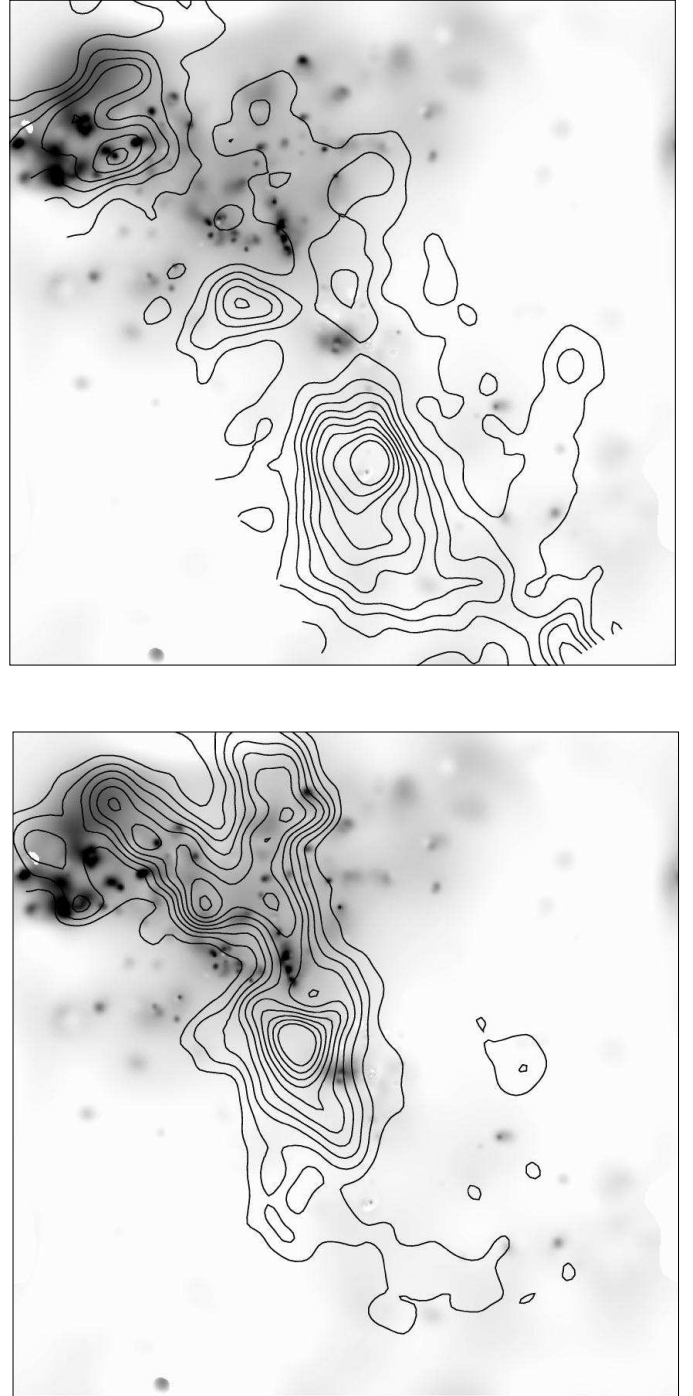


Fig. 3. Contour lines of the $6.1 \text{ mm CS } J = 1 \rightarrow 0$ line emission in the velocity ranges $(10-30) \text{ km s}^{-1}$ (top) and $(40-50) \text{ km s}^{-1}$ (bottom), superimposed on a grayscale equivalent-width image of the 6.4 keV low-ionization $\text{Fe K}\alpha$ line emission, in a $17' \times 17'$ field of view centered on Sgr A*. The CS data are from Tsuboi et al. (1999) and the 6.4 keV data from Park et al. (2004). Figure credit: Sangwook Park.

ing at $(\Delta\alpha, \Delta\delta) \approx (3'.0, 1'.5)$ with respect to Sgr A* and a molecular ridge curving all the way around the eastern edge of the Sgr A East radio shell. As noted earlier by other authors, this spatial configuration strongly suggests that Sgr A East is colliding with, and compressing, M-0.02-0.07. Serabyn et al. (1992) found that radial velocities in M-0.02-0.07 peak at $\approx 45 \text{ km s}^{-1}$ and span the range $\approx (25 - 65) \text{ km s}^{-1}$, with a steady increase

⁵ The designation Sgr A East Core was taken up by Mezger et al. (1996). However, instead of envisioning an extended M-0.02-0.07 that would contain the entire Sgr A East Core (in addition to the Curved Streamer), they regarded M-0.02-0.07 as being only "the compressed eastern part of the Sgr A East Core".

from south to north along the ridge. They argued that this velocity gradient is intrinsic to the cloud, and not caused by its interaction with Sgr A East. From the measured CS ($7 \rightarrow 6$)-to- $(5 \rightarrow 4)$ line ratio, they derived a true H_2 density $\approx (1-2) \times 10^6 \text{ cm}^{-3}$, and from the CS velocity-integrated line intensities, they derived a space-averaged H_2 density $\approx 3 \times 10^4 \text{ cm}^{-3}$ near the emission peak and lower by up to a factor ≈ 2 in the ridge (assuming a line-of-sight depth $\approx 2.5 \text{ pc}$) as well as a hydrogen mass $\approx 1.5 \times 10^5 M_\odot$ for the entire cloud.

In contrast to Zylka et al. (1990), who viewed the Curved Streamer (their ^{13}CO counterpart of the CS ridge) as a northward extension of M-0.13-0.08, separate from the Sgr A East Core, Serabyn et al. (1992) concluded that the CS ridge is truly part of M-0.02-0.07 and in physical contact with Sgr A East, while being separate from M-0.13-0.08. Moreover, since they observed both highly blue- and redshifted gas just inside of the compressed CS ridge, which they identified with gas accelerated by the expansion of Sgr A East, they concluded that molecular gas must be present on both the near and far sides of Sgr A East (although with asymmetric distributions in favor of the far side). In other words, the gas-and-dust shell surrounding Sgr A East may be thinner (as suggested by Mezger et al. 1989), but not completely open, toward the Sun.

Yet another perspective emerges from the work of Coil & Ho (1999, 2000), who observed the central $10 \text{ pc} \times 15 \text{ pc}$ of the Galaxy in the NH_3 (J, K) = (1, 1) and (2, 2) transitions (both around 23.7 GHz). Aside from an incomplete ring of emission corresponding to the CNR, they clearly saw two long and narrow molecular streamers located to the south and east, respectively, of Sgr A* and running roughly parallel to the Galactic plane. Coil & Ho (1999) focused on the Southern Streamer and Coil & Ho (2000) on the Eastern Streamer, which they also called the Molecular Ridge.

The Southern Streamer, which is $\approx 10 \text{ pc} \times 2 \text{ pc}$ in projection, appears to connect the northern edge of the 20 km s^{-1} cloud to the southeastern part of the CNR (Coil & Ho 1999). Its bulk radial velocity is $\approx (20 - 35) \text{ km s}^{-1}$, with a systematic increase toward the CNR, while its velocity dispersion is $\approx (30 - 40) \text{ km s}^{-1}$, with an abrupt jump to $\geq 50 \text{ km s}^{-1}$ near the CNR. The gas kinetic temperature is $\approx (17 - 35) \text{ K}$ in most of the streamer and jumps to $\approx 300 \text{ K}$ at its northern tip. Taken together, these morphological, kinematic and thermal properties provide good evidence that the Southern Streamer is feeding the CNR with molecular gas from the 20 km s^{-1} cloud – as suggested before by Okumura et al. (1991). In this scenario, the northward velocity gradient measured along the Southern Streamer automatically positions the 20 km s^{-1} cloud in front of the CNR. As seen in NH_3 emission, the Southern Streamer has a hydrogen mass $\sim 3.5 \times 10^5 M_\odot$ and, assuming a line-of-sight depth $\approx 2 \text{ pc}$, a space-averaged H_2 density $\sim (1 - 2) \times 10^5 \text{ cm}^{-3}$. For comparison, the true H_2 densities traced by the NH_3 (1, 1) and (2, 2) transitions are typically a few 10^5 cm^{-3} .

The Eastern Streamer, or Molecular Ridge, which is somewhat longer ($\geq 12 \text{ pc}$) in projection than the Southern Streamer, appears to trace the denser parts of the 50 km s^{-1} cloud (Coil & Ho 2000). Its northern half wraps around the eastern edge of Sgr A East, while its southern half continues past Sgr A East toward the 20 km s^{-1} cloud. Its bulk radial velocity globally jumps from $\approx 40 \text{ km s}^{-1}$ in the northern half to $\approx 20 \text{ km s}^{-1}$ in the southern half, with a general tendency to increase westward in the northern half and eastward in the southern half. However, there are regions in the northern half which display both blue- and (brighter) redshifted emission, suggesting that the Molecular Ridge contains gas both in front of and (in greater amounts)

behind Sgr A East. The velocity dispersion, too, has a discontinuous behavior: it turns from roughly uniform in the northern half, consistent with the gas being processed and postshock, to highly variable in the southern half, consistent with the gas being strongly perturbed by the G359.92-0.09 SNR to the south of Sgr A East. This SNR appears to be also interacting with Sgr A East, producing a noticeable inward bend in its southern boundary, and with the 20 km s^{-1} cloud, making its eastern edge sharp and straight. Since the SNR is ≈ 3.5 (9 pc) in size, these simultaneous interactions imply that the 20 km s^{-1} cloud must be less than $\approx 9 \text{ pc}$ away from (i.e., in front of) Sgr A East. As seen in NH_3 emission, the Molecular Ridge has a hydrogen mass $\sim 1.5 \times 10^5 M_\odot$, with $\sim 1.1 \times 10^5 M_\odot$ in the northern half and $\sim 0.4 \times 10^5 M_\odot$ in the southern half, and a space-averaged H_2 density $\sim (1 - 2) \times 10^5 \text{ cm}^{-3}$, assuming again a line-of-sight depth $\approx 2 \text{ pc}$.

A follow-up study of the central 10 pc of the Galaxy was performed by McGary et al. (2001), based on spectral observations of the NH_3 (1, 1), (2, 2) and (3, 3) transitions (all between 23.7 GHz and 23.9 GHz). In addition to the Southern Streamer and the Molecular Ridge clearly visible in the (1, 1) and (2, 2) maps of Coil & Ho (1999, 2000), the (3, 3) map brings out two new features:

- The Western Streamer, located west of Sgr A*, extends in the north-south direction over ≈ 2.8 (7 pc). It closely follows the western boundary of Sgr A East, suggesting that it is made of material swept up by the expansion of the SNR. Its bulk radial velocity gradually increases from $\approx -70 \text{ km s}^{-1}$ near its southern tip to $\approx +90 \text{ km s}^{-1}$ near its northern tip. This large velocity gradient could be due to intrinsic rotation or to orbital motion around Sgr A*, with a possible enhancement by the expansion of Sgr A East.
- The Northern Ridge, located northeast of Sgr A*, extends in the northeast-southwest direction over ≈ 1.4 (3.5 pc). It lies along the northern boundary of Sgr A East, so it, too, could be made of swept-up material. Its bulk radial velocity is $\approx -10 \text{ km s}^{-1}$ all along, and it is kinematically connected to the northeastern lobe of the CNR through a narrow streamer along which the radial velocity increases smoothly from $\approx -10 \text{ km s}^{-1}$ to $\approx +60 \text{ km s}^{-1}$. If this kinematic connection represents inflow toward the CNR, the Northern Ridge must be slightly in front of the northeastern lobe of the CNR, and Sgr A East itself must be close to the CNR.

Herrnstein & Ho (2005) pursued McGary et al.'s (2001) study after adding to their NH_3 (1, 1), (2, 2) and (3, 3) data the 25 GHz NH_3 (6, 6) data of Herrnstein & Ho (2002). Assuming an NH_3 -to- H_2 ratio of 10^{-7} (as opposed to 10^{-8} in Coil & Ho 1999, 2000), they estimated the H_2 masses of the major molecular clouds at roughly $\geq 8 \times 10^4 M_\odot$ for the Southern Streamer, $\geq 3 \times 10^4 M_\odot$ for the Molecular Ridge, $\geq 5 \times 10^4 M_\odot$ for the core of the 50 km s^{-1} cloud, $\sim 4 \times 10^3 M_\odot$ for the Western Streamer and $\sim 2 \times 10^3 M_\odot$ for the Northern Ridge. Note that the first three values only give lower limits because the associated objects extend past the edge of the NH_3 maps – this is particularly true of the core of the 50 km s^{-1} cloud, which has roughly three-quarters of its projected volume outside the maps, so that its total mass could actually be as large as $\sim 2 \times 10^5 M_\odot$. Herrnstein & Ho (2005) also found the molecular gas to have a two-temperature structure on scales $\lesssim 0.5 \text{ pc}$, with $\sim 75\%$ of the gas at $\lesssim 25 \text{ K}$ (probably $\sim 15 \text{ K}$) and $\sim 25\%$ at $\sim 200 \text{ K}$.

By considering their NH_3 data in conjunction with existing data at other frequencies, Herrnstein & Ho (2005) developed a three-dimensional picture for the spatial arrangement of the main molecular features within a few pc of the GC. In this picture, Sgr A*, Sgr A West and the surrounding CNR reside just in-

side the near surface of Sgr A East; the 20 km s^{-1} cloud and the Southern Streamer lie entirely in front of Sgr A East; the 50 km s^{-1} cloud envelops Sgr A East from front to back along its eastern side, and it is connected to the 20 km s^{-1} cloud by the Molecular Ridge. These line-of-sight positions are consistent with the observational results presented above as well as with the finding that the 20 km s^{-1} cloud strongly absorbs the $(2-10) \text{ keV}$ X-ray emission from the central $17'$, while the 50 km s^{-1} cloud does not (Park et al. 2004). Furthermore, from the ≈ -70 to $+90 \text{ km s}^{-1}$ velocity gradient along the Western Streamer and the $\approx -10 \text{ km s}^{-1}$ velocity all along the Northern Ridge measured by McGary et al. (2001), Herrnstein & Ho (2005) concluded that the Western Streamer is highly inclined to the plane of the sky, with its southern part on the front side and its northern part on the back side of Sgr A East,⁶ while the Northern Ridge is roughly parallel to the plane of the sky, at about the line-of-sight distance of Sgr A East's center.

The three-dimensional picture of Herrnstein & Ho (2005) was later modified by Lee et al. (2008), who carried out spectral observations of the $2.12 \mu\text{m}$ $\text{H}_2 \nu = 1 - 0 \text{ S}(1)$ emission line in four areas along the periphery of Sgr A East, where the shock front is expanding in molecular clouds. In contrast to NH_3 emission, which traces cool ($T \lesssim 100 \text{ K}$) molecular gas, H_2 emission traces hot ($T \sim 2000 \text{ K}$) molecular gas and is, therefore, ideally suited to probe shock-heated molecular regions. Thus Lee et al. (2008) compared position-velocity diagrams of H_2 emission (assumed to trace postshock gas) and NH_3 emission (assumed to trace preshock gas) to derive shock velocities and use them as indicators of line-of-sight positions relative to the center of Sgr A East. As a general rule, they found that the H_2 lines are much broader and either blue- or redshifted with respect to the corresponding NH_3 lines. They concluded that Sgr A East is driving shocks into, and hence is in physical contact with, each of the 50 km s^{-1} cloud, the Molecular Ridge (at least its northern part), the Northern Ridge, the Western Streamer, the Southern Streamer and the CNR. More specifically, they gathered that the 50 km s^{-1} cloud brackets the eastern part of Sgr A East along the line of sight; the Molecular Ridge probably lies between the front and back sides of Sgr A East, with its northern end slightly tipped toward the back; the Northern Ridge lies to the back side of Sgr A East; the northern half of the Western Streamer surrounds the western edge of Sgr A East from front to back; the Southern Streamer and the CNR lie in front of Sgr A East. They also confirmed earlier claims that the Molecular Ridge connects the 20 km s^{-1} and 50 km s^{-1} clouds, while the Southern Streamer connects the 20 km s^{-1} cloud to the CNR.

Amo-Baladrón et al. (2011) obtained complementary information on the three-dimensional disposition of molecular features in the central 12 pc and on their possible connections by comparing the emissions from selected molecular tracers believed to respond differently to interstellar shocks and to UV radiation. Their data set comprises their own measurements of $\text{SiO } J = 2 \rightarrow 1$ (tracer of shocked gas), $\text{HNCO } J = 5_{0,5} \rightarrow 4_{0,4}$ (tracer of shocked gas, very sensitive to photo-dissociation), $\text{H}^{13}\text{CO}^+ J = 1 \rightarrow 0$ (similar to SiO) and $\text{HN}^{13}\text{C } J = 1 \rightarrow 0$ (similar to HNCO), in addition to Tsuboi et al.'s (1999) measurements of $\text{CS } J = 1 \rightarrow 0$ (tracer of quiescent dense gas).

⁶ This interpretation raises a self-consistency problem. If the Western Streamer is indeed swept-up material at the surface of Sgr A East, the mere fact that it runs precisely along the projected boundary of Sgr A East provides strong evidence that it is approximately contained in the sky plane through the center of Sgr A East. This line-of-sight position is supported by the conclusions of Lee et al. (2008) (see below in Section 2.5).

They used the HNCO-to-SiO , SiO-to-CS and HNCO-to-CS intensity ratios as indicators of relative distances to the central star cluster (the source of the UV radiation responsible for photo-dissociation) and of the presence of gas shocked by the expansion of Sgr A East. In this manner, they found that the Molecular Ridge is probably relatively distant from the central cluster or else shielded from its UV photons; the Northern Ridge is close to the central cluster and possibly connected to the northeastern part of the CNR; the Southern Streamer approaches the central cluster going northward and probably connects the 20 km s^{-1} cloud to the southeastern part of the CNR; the Western Streamer is close to the central cluster and was swept up by the Sgr A East shock.

It is important to emphasize that the relative line-of-sight locations of the main interstellar objects near the GC are still a matter of controversy. For instance, the 18 cm spectral observations of the four OH ground-state transitions by Karlsson et al. (2003) showed strong absorption against the eastern and most of the western parts of the Sgr A East shell, but a lack of absorption against the spiral pattern of the Sgr A West H II region. This prompted the authors to suggest that a fraction of the molecular belt (comprising the 20 km s^{-1} and 50 km s^{-1} clouds) lies in front of Sgr A East and, at the same time, behind Sgr A West, so that both radio sources must be separated by a finite distance along the line of sight. Obviously, this view contradicts the notion that Sgr A West is embedded within Sgr A East (e.g., Yusef-Zadeh et al. 2000; Maeda et al. 2002). Similarly, the 1720 MHz OH absorption measurements of Sjouwerman & Pihlström (2008) indicated that the 20 km s^{-1} and 50 km s^{-1} clouds lie mostly behind Sgr A West and at least partly in front of Sgr A East. Incidentally, both Karlsson et al. (2003) and Sjouwerman & Pihlström (2008) were able to clearly identify the CNR in OH absorption at high absolute velocities, thereby confirming its location on the near side of Sgr A East.

3. Our representation of the interstellar gas

Now armed with all the observational results described in Section 2, we proceed to construct a plausible and handy (as far as possible) representation of the interstellar gas within $\sim 10 \text{ pc}$ of Sgr A*. Unless stated otherwise, the parameter values adopted in the following subsections are based on the observational studies discussed in the corresponding subsections of Section 2 and on complementary theoretical arguments made both to fill in the gaps in the observational estimates and to ensure self-consistency of our gas representation. For convenience, a summary of our adopted values for the geometrical and thermodynamic parameters of the different structural components is given in Tables 1 and 2. In addition, three orthogonal (front, side and top) views showing the spatial organization of the different components, with their respective shapes and relative sizes, are schematically drawn in Figure 4.

3.1. The Central Cavity

We approximate the Central Cavity as an ellipsoid centered on Sgr A*, axisymmetric about the vertical axis and having dimensions $l_x \times l_y \times l_z = 2.9 \text{ pc} \times 2.9 \text{ pc} \times 2.1 \text{ pc}$, where l_y and l_z correspond to the projected *FWHM* dimensions of the extended radio component discussed by Beckert et al. (1996). The volume of the Central Cavity is then $V_{\text{cc}} = 9.2 \text{ pc}^3$. We consider that the Central Cavity contains warm ionized gas, divided between an extended (or diffuse) component and the Minispiral, neutral atomic gas, confined to one or two neutral streamers,

Table 1. Geometrical parameters of the different structural components in our representation of the interstellar gas.

Component	Shape	Dimensions [pc] ^a	Volume [pc ³]	Position [pc] ^b
Central Cavity (CC)	ellipsoid	$l_x \times l_y \times l_z = 2.9 \times 2.9 \times 2.1$	9.2	centered on Sgr A*
Extended component			8.4	
Minispiral		$l = 9.7$ & $d = 0.1$	0.076	
Neutral streamers		$l = 6.2$ & $d = 0.3$	0.44	
Central sphere		$d = 0.8$	0.27	
Circumnuclear Ring (CNR)	trapezoidal ring	$r_{\text{in}} = 1.2, r_{\text{out}} = 3.0$ & $h_{\text{in}} = 0.4, h_{\text{out}} = 1.0$	18	centered on Sgr A*
Main molecular ring		$r_{\text{in}} = 1.2, r_{\text{out}} = 3.0$	18	
Photo-dissociated inner layer		$r_{\text{in}} = 1.2, r_{\text{out,a}} = 1.6$	1.65	
Sgr A East SNR	ellipsoid	$L_x \times L_y \times L_z = 9.0 \times 9.0 \times 6.7$	285	$(x_c, y_c, z_c) = (-2.0, 1.2, -1.5)$
Extended component			260	
Radio halo	sphere	$d = 18$	3 050	$(x_c, y_c, z_c) = (-2.0, 1.2, -1.5)$
Extended component			2 440	
Belt of molecular clouds ^{c,d}				
M-0.13-0.08 (SC)	ellipsoid	$\ell_x \times \ell_y \times \ell_z = 7.5 \times 15 \times 7.5$	442	$(x_{\text{SC}}, y_{\text{SC}}, z_{\text{SC}}) = (4 - 12, -11, -5)$
M-0.02-0.07 (EC)	indented sphere	$d = 9$	356	$(x_{\text{EC}}, y_{\text{EC}}, z_{\text{EC}}) = (-3, 7, -4.5)$
Preshock core			305	
Swept-up shell		$\Delta r = 1.5$	51	along NE bdy of SNR
Molecular Ridge (MR)			79 - 98	
Swept-up shell		$\Delta r = 1.5$	51	along NE bdy of SNR
Bridge	curved cylinder	$l = (9 - 15)$ & $d = 2$	28 - 47	between EC & SC
Southern Streamer (SS)	curved cylinder	$l = (7 - 14)$ & $d = 2$	22 - 44	between SC & CNR
Western Streamer (WS)	curved cylinder	$l = 8$ & $d = 1$	6	along W bdy of SNR
Northern Ridge (NR)	curved cylinder	$l = 4$ & $d = 1$	3	along N bdy of SNR

^a The errors in our adopted dimensions, which arise from observational uncertainties and from our geometrical approximations, are estimated as follows [in pc]: Central Cavity: $\delta l_y \approx \delta l_z \approx 0.5$. Minispiral: $\delta l \approx 4, \delta d \approx \begin{smallmatrix} +0.1 \\ -0.05 \end{smallmatrix}$. Neutral streamers: $\delta l \approx 3, \delta d \approx 0.15$. Central sphere: $\delta d \approx 0.4$. CNR: $\delta r_{\text{in}} \approx 0.4, \delta r_{\text{out}} \approx \begin{smallmatrix} +4 \\ -0.5 \end{smallmatrix}, \delta h_{\text{in}} \approx 0.2, \delta h_{\text{out}} \approx 0.5$. Sgr A East: $\delta L_y \approx \delta L_z \approx 1.5$. Radio halo: $\delta d \approx 5$. M-0.13-0.08: $\delta \ell_y \approx \delta \ell_z \approx 3$. M-0.02-0.07: $\delta d \approx 3$. Swept-up shell: $\delta \Delta r \approx 0.7$. Bridge and Southern Streamer: $\delta d \approx 1$. Western Streamer and Northern Ridge: $\delta l \approx 2, \delta d \approx 0.5$.

^b The errors in our adopted positions are estimated as follows [in pc]: ≈ 0.1 for the Central Cavity; ≈ 0.3 for the CNR and Sgr A East; ~ 2 for the radio halo and the different molecular clouds in the belt.

^c The swept-up shell is indicated twice, because it is part of both M-0.02-0.07 and the Molecular Ridge.

^d The ranges given for the lengths and volumes of the Bridge (and hence the Molecular Ridge) and the Southern Streamer correspond to the range in the line-of-sight coordinate of the center of M-0.13-0.08, x_{SC} .

and hot ionized gas, extending over the central 0.8 pc. For simplicity, we ignore the fine-scale structure observed in each of these gas components (including the Minicavity, stellar winds, dense clumps, etc.), which we take to be smooth and homogeneous. We set the temperatures of the three gases to $T_{\text{wi}} = 7\,000$ K (Roberts & Goss 1993; Shukla et al. 2004), $T_a = 170$ K (Jackson et al. 1993) and $T_h = 1.5 \times 10^7$ K (Baganoff et al. 2003), and we consider that the warm ionized gas has hydrogen completely ionized and helium completely neutral, while the hot ionized gas has both hydrogen and helium fully ionized.

The extended component of the warm ionized gas is supposed to have a central emission measure of 2.2×10^6 pc cm⁻⁶ (value derived by Beckert et al. (1996) and scaled up to our adopted temperature), which, combined with a line-of-sight dimension $l_x = 2.9$ pc and a filling factor ϕ_{ext} , yields a true electron density $(n_e)_{\text{ext}} = (870 \text{ cm}^{-3}) \phi_{\text{ext}}^{-1/2}$ and a space-averaged electron density $\langle n_e \rangle_{\text{ext}} = (870 \text{ cm}^{-3}) \phi_{\text{ext}}^{1/2}$. Since all the free electrons are presumed to come from hydrogen, the H⁺ density is simply $n_{\text{H}^+} = n_e$ and the H⁺ mass of the extended component $(M_{\text{H}^+})_{\text{ext}} = (200 M_\odot) \phi_{\text{ext}}^{1/2}$. The reason why our electron densities and H⁺ mass differ somewhat from those derived by Beckert et al. (1996) is not only because we adopted a higher temperature, but also, and more importantly, because we as-

sumed an ellipsoidal cavity with a central line-of-sight depth of 2.9 pc, whereas they assumed a constant line-of-sight depth ≈ 1 pc.

The parameters of the Minispiral are more uncertain. Here, we consider that the Minispiral is composed of three arms: the Northern Arm, the Eastern Arm + Bar and the Western Arc. We furthermore assume that the three arms follow the Keplerian elliptical orbits derived by Zhao et al. (2009) – in a particularly careful analysis based on a combination of proper motion and radial velocity measurements – and rescaled to $r_\odot = 8.5$ kpc (see their Table 5 for a list of all the orbital parameters), that they are, respectively, 2.7 pc, 3.5 pc and 3.5 pc long (as calculated from the ranges of true anomaly quoted by Zhao et al. 2009) and that they all have a circular cross-section of diameter (0.1 pc) $d_{0.1}$. Under these conditions, the total length of the Minispiral is 9.7 pc and its total volume $V_{\text{msp}} = (0.076 \text{ pc}^3) d_{0.1}^2$. We note that the total length of 9.7 pc obtained here is significantly greater than the total length of 3.9 pc measured by Shukla et al. (2004), which is mainly because the latter is a two-dimensional length in the plane of the sky, as opposed to a full three-dimensional length.

Once the volume of the Minispiral has been determined, its electron density and H⁺ mass can be inferred from its measured radio emission flux density. Indeed, for a warm ionized

Table 2. Thermodynamic parameters (interstellar phase, temperature, mean hydrogen density and hydrogen mass) of the different structural components in our representation of the interstellar gas.

Component	Phase	T [K] ^a	n_{H} [cm ⁻³] ^b	M_{H} [M_{\odot}] ^c
Central Cavity (CC)				
Extended component	warm ionized	7 000	910	190
Minispiral	warm ionized	7 000	6 200	12
Neutral streamers	atomic	170	1.5×10^4	160
Central sphere	hot ionized	1.5×10^7	18.5	0.12
Circumnuclear Ring (CNR)				
Main molecular ring	molecular	150	4.4×10^5	2×10^5
Photo-dissociated inner layer	atomic	300	3.2×10^4	1 300
Sgr A East SNR				
Extended component	hot ionized	1.5×10^7	3.0	19
Radio halo				
Extended component	warm ionized	7 000	210	1.3×10^4
Belt of molecular clouds ^{d,e}				
M-0.13-0.08 (SC)	molecular	60	2×10^4	2.2×10^5
M-0.02-0.07 (EC)	molecular	60		1.9×10^5
Preshock core			2×10^4	1.5×10^5
Swept-up shell			3×10^4	3.8×10^4
Molecular Ridge (MR)	molecular	60	3×10^4	$(5.9 - 7.3) \times 10^4$
Swept-up shell				3.8×10^4
Bridge				$(2.1 - 3.5) \times 10^4$
Southern Streamer (SS)	molecular	60	3×10^4	$(1.6 - 3.2) \times 10^4$
Western Streamer (WS)	molecular	60	3×10^4	4.5×10^3
Northern Ridge (NR)	molecular	60	3×10^4	2.2×10^3

^a The actual temperature ranges, accounting for observational uncertainties, model approximations and true physical dispersion, are [in K]: Central Cavity: $\approx (5\,000 - 13\,000)$ for the warm ionized gas; $\approx (100 - 240)$ for the atomic gas; $\approx (1.4 - 2.3) \times 10^7$ for the hot ionized gas. CNR: $\approx (40 - 300)$ for the molecular gas; $\approx (200 - 1\,000)$ for the atomic gas. Sgr A East: $\approx (1 - 7) \times 10^7$. Radio halo: $\approx (5\,000 - 10\,000)$. Belt of molecular clouds: $\approx (15 - 200)$.

^b The actual hydrogen density ranges, accounting for observational uncertainties, model approximations and true physical dispersion, are [in cm⁻³]: Central Cavity: $\approx (10^3 - 2 \times 10^5)$ for the warm ionized gas; $\approx (2 \times 10^3 - 3 \times 10^5)$ for the atomic gas; $\approx (10 - 40)$ for the hot ionized gas. CNR: $\approx (10^4 - 2 \times 10^8)$ for the molecular gas; $\approx (10^4 - 2 \times 10^5)$ for the atomic gas. Sgr A East: $\approx (1.5 - 30)$. Radio halo: $\approx (10 - 1\,000)$. Belt of molecular clouds: $\approx (10^4 - 4 \times 10^6)$.

^c The errors in our adopted masses are estimated as follows: a factor ~ 4 for the ionized components (including uncertainties in the observed emission measures, in the projected surface areas and in the line-of-sight depths); a factor ~ 5 for the atomic and molecular components (including uncertainties in the measured column densities, in the tracer-to-hydrogen ratios and in the projected surface areas). For the radio halo, the error is in fact larger than a factor ~ 4 , as the relative contribution from warm ionized gas to the observed radio emission is itself very uncertain.

^d The swept-up shell is indicated twice, because it is part of both M-0.02-0.07 and the Molecular Ridge.

^e The mass ranges given for the Bridge (and hence the Molecular Ridge) and the Southern Streamer correspond to the range in the line-of-sight coordinate of the center of M-0.13-0.08, $x_{\text{SC}} = (4 - 12)$ pc.

gas component (with given electron temperature and ionization state) occupying a volume V , within which its filling factor is ϕ , and producing thermal free-free emission with flux density F_{ν} , the true electron density and H^+ mass scale roughly as $n_{\text{e}} \propto [F_{\nu}/(V\phi)]^{1/2}$ and $M_{\text{H}^+} \propto [F_{\nu}(V\phi)]^{1/2}$. Beckert et al. (1996), who tried to separate the Minispiral from the extended component in a 2 cm continuum map of Sgr A West, estimated their contributions to the 2 cm flux density at $(F_{\nu})_{\text{ext}} = 19$ Jy and $(F_{\nu})_{\text{msp}} = 8$ Jy. For the effective volumes, we have $(V\phi)_{\text{ext}} = (9.2 \text{ pc}^3) \phi_{\text{ext}}$ and $(V\phi)_{\text{msp}} = (0.076 \text{ pc}^3) d_{0.1}^2 \phi_{\text{msp}}$. We also know that the extended component has $(n_{\text{e}})_{\text{ext}} = (870 \text{ cm}^{-3}) \phi_{\text{ext}}^{-1/2}$ and $(M_{\text{H}^+})_{\text{ext}} = (200 M_{\odot}) \phi_{\text{ext}}^{1/2}$. It then follows that the Minispiral must have $(n_{\text{e}})_{\text{msp}} = (6\,200 \text{ cm}^{-3}) d_{0.1}^{-1} \phi_{\text{msp}}^{-1/2}$ and $(M_{\text{H}^+})_{\text{msp}} = (12 M_{\odot}) d_{0.1} \phi_{\text{msp}}^{1/2}$. For $d_{0.1} = 1$ (Beckert et al. 1996; Shukla et al. 2004) and $\phi_{\text{msp}} = 1$, the volume, (true or space-averaged) electron density and H^+ mass of the Minispiral reduce to $V_{\text{msp}} =$

0.076 pc^3 , $(n_{\text{e}})_{\text{msp}} = 6\,200 \text{ cm}^{-3}$ and $(M_{\text{H}^+})_{\text{msp}} = 12 M_{\odot}$.⁷ The density and mass are reasonably close to those obtained by Beckert et al. (1996), and the differences can mostly be explained by our using the full three-dimensional length of the Minispiral, instead of its two-dimensional length in the plane of the sky. If we now split the H^+ mass of the Minispiral into its three arms according to their respective lengths, we find $3.4 M_{\odot}$ in the Northern Arm, $4.3 M_{\odot}$ in the Eastern Arm + Bar and $4.3 M_{\odot}$ in the Western Arc.

Neutral atomic gas inside the Central Cavity resides either in one large neutral streamer, the so-called Northern Streamer, bounded by the ionized Northern and Eastern Arms

⁷ These values refer to the ionized gas traced by the 2 cm continuum emission. It is, therefore, not surprising that the density derived here is lower than the density inferred from emission at millimeter wavelengths (Shukla et al. 2004; Zhao et al. 2010), which refers to a denser ionized gas component.

of the Minispiral (Jackson et al. 1993), or in two thinner neutral streamers, adjacent to the Northern and Eastern Arms, respectively (Latvakoski et al. 1999). Because the Northern and Eastern Arms turn out to be on nearly perpendicular orbits (Zhao et al. 2010), it is hard to imagine that they could be linked to the same neutral streamer, which leads us to opt for the second possibility and follow Latvakoski et al. (1999). Nonetheless, to ensure self-consistency in our gas representation, we do not strictly stick to their dust model, which places the neutral streamers on parabolic orbits about Sgr A*. Instead, we consider that the neutral streamers run exactly alongside their ionized counterparts (themselves on Keplerian elliptical orbits; see above), on their sides farther from Sgr A*. The neutral streamer associated with the Northern Arm is then 2.7 pc long and that associated with the Eastern Arm + Bar 3.5 pc long. Next, we assume that both neutral streamers have a circular cross-section of diameter 0.3 pc, which corresponds to their projected thickness in the far-infrared maps of Latvakoski et al. (1999), and we assign them the H I masses derived by Latvakoski et al. (1999). Thus we find that the neutral streamer associated with the Northern Arm has a volume of 0.19 pc^3 , an H I mass of $110 M_\odot$, and hence a mean H I density of $2.3 \times 10^4 \text{ cm}^{-3}$, while the neutral streamer associated with the Eastern Arm + Bar has a volume of 0.25 pc^3 , an H I mass of $50 M_\odot$, and hence a mean H I density of $8 \times 10^3 \text{ cm}^{-3}$. Together, the two neutral streamers occupy a volume $V_{\text{nstr}} = 0.44 \text{ pc}^3$, enclose an H I mass $(M_{\text{H I}})_{\text{nstr}} = 160 M_\odot$ and have a mean H I density $\langle n_{\text{H I}} \rangle_{\text{nstr}} = 1.5 \times 10^4 \text{ cm}^{-3}$. It is important to realize that the above mean H I densities represent spatial averages over the neutral streamers, whereas the space-averaged H I density $\approx 1.6 \times 10^3 \text{ cm}^{-3}$ derived by Jackson et al. (1993) refers to a spatial average over the Central Cavity. Furthermore, if the true H I density $\approx 3 \times 10^5 \text{ cm}^{-3}$ derived by Jackson et al. (1993) is characteristic, the implied mean filling factor of [O I]-emitting atomic gas within the neutral streamers is ~ 0.05 .

Finally, for the hot ionized gas, we follow Baganoff et al. (2003) and assume that this gas is contained within a centered sphere of radius 0.4 pc, and hence volume $V_{\text{hot}} = 0.27 \text{ pc}^3$, that it is fully ionized, with twice solar abundances, and that it has a true electron density $(n_e)_h = (26 \text{ cm}^{-3}) \phi_h^{-1/2}$. Under these conditions, its true H^+ density is $(n_{\text{H}^+})_h = \frac{1}{1.4} (n_e)_h = (18.5 \text{ cm}^{-3}) \phi_h^{-1/2}$ and its H^+ mass $(M_{\text{H}^+})_{\text{hot}} = (0.12 M_\odot) \phi_h^{1/2}$. To determine the filling factor ϕ_h , we consider the assumption of rough thermal pressure balance between the extended warm ionized gas and the hot ionized gas, such that $2.2 (n_{\text{H}^+})_{\text{ext}} T_{\text{wi}} \approx 2.6 (n_{\text{H}^+})_h T_h$. With $T_{\text{wi}} = 7000 \text{ K}$, $T_h = 1.5 \times 10^7 \text{ K}$ (see beginning of Section 3.1), $(n_{\text{H}^+})_{\text{ext}} = (870 \text{ cm}^{-3}) \phi_{\text{ext}}^{-1/2}$ and $(n_{\text{H}^+})_h = (18.5 \text{ cm}^{-3}) \phi_h^{-1/2}$, thermal pressure balance would imply $\phi_h \gg \phi_{\text{ext}}$, which is impossible.⁸ In consequence, both gases cannot be in thermal pressure balance, and the overpressured hot ionized gas will tend to completely fill the central 0.4 pc radius sphere. In other words, we may take $\phi_h = 1$ inside the central sphere, whereupon the (true or space-averaged) H^+ density and H^+ mass of hot ionized gas become $(n_{\text{H}^+})_h = 18.5 \text{ cm}^{-3}$ and $(M_{\text{H}^+})_{\text{hot}} = 0.12 M_\odot$.

We can now complete our specification of the parameters of the extended warm ionized gas. The volume left to this com-

ponent is the volume inside the Central Cavity that is not occupied by either the Minispiral or the neutral streamers or the central sphere, i.e., $V_{\text{ext}} = V_{\text{cc}} - V_{\text{msp}} - V_{\text{nstr}} - V_{\text{hot}} = 8.4 \text{ pc}^3$, and the associated filling factor within the Central Cavity is $\phi_{\text{ext}} = V_{\text{ext}}/V_{\text{cc}} = 0.91$. It then follows that the extended warm ionized gas has a true H^+ density $(n_{\text{H}^+})_{\text{ext}} = 910 \text{ cm}^{-3}$, a space-averaged H^+ density $\langle n_{\text{H}^+} \rangle_{\text{ext}} = 830 \text{ cm}^{-3}$ and an H^+ mass $(M_{\text{H}^+})_{\text{ext}} = 190 M_\odot$.

3.2. The Circumnuclear Ring

Although all observations point to a highly irregular and clumpy structure, which extends significantly farther out to the southwest than to the northeast, for simplicity we model the CNR as a well-defined, smooth and axisymmetric ring. We consider that this ring is centered on Sgr A* (thus ignoring the slight south-east offset mentioned by Güsten et al. 1987) and that it extends radially from $r_{\text{in}} = 1.2 \text{ pc}$ (Güsten et al. 1987; Christopher et al. 2005) to $r_{\text{out}} = 3.0 \text{ pc}$. These values are a compromise between the various estimates found in the literature: $0.8 \text{ pc} \leq r_{\text{in}} \leq 1.4 \text{ pc}$ (Wright et al. 2001; Genzel et al. 1985), $2.5 \text{ pc} \leq r_{\text{out}} \leq 2.7 \text{ pc}$ to the northeast (Wright et al. 2001; Christopher et al. 2005; Güsten et al. 1987) and $4.2 \text{ pc} \leq r_{\text{out}} \leq 7 \text{ pc}$ to the southwest (Güsten et al. 1987; Serabyn et al. 1986). We also assume that the CNR has a trapezoidal cross-section, with axial thickness increasing from $h(r_{\text{in}}) = 0.4 \text{ pc}$ to $h(r_{\text{out}}) = 1.0 \text{ pc}$ (in accordance with the inner value and the slope derived by Güsten et al. 1987). The volume of the CNR is then $V_{\text{CNR}} = 18 \text{ pc}^3$. Lastly, we take the plane of the CNR to lie at inclination 70° to the plane of the sky (Genzel et al. 1985; Jackson et al. 1993) and to intersect the latter at position angle 25° east of north (Jackson et al. 1993), i.e., somewhat less than the position angle $31^\circ 40'$ of the Galactic plane.

It is interesting to note that the inner radius of the CNR ($r_{\text{in}} = 1.2 \text{ pc}$) is somewhat smaller than the horizontal radius of the Central Cavity ($l_x/2 = 1.45 \text{ pc}$), so that the CNR slightly encroaches upon the Central Cavity. On the other hand, the inner radius of the CNR coincides exactly with the semimajor axis of the nearly circular Western Arc ($a = 1.2 \text{ pc}$; see Zhao et al. 2009) and both structures have comparable inclinations (70° and 63° , respectively), consistent with the Western Arc being the ionized inner edge of the western portion of the CNR.

The molecular gas density inside the CNR varies over orders of magnitude, as revealed by the widely different values inferred from different tracers. Typically, rotational lines of CO, CS, and HCN or HCO^+ yield true H_2 densities of a few 10^4 cm^{-3} (Harris et al. 1985; Sutton et al. 1990; Bradford et al. 2005), a few 10^5 cm^{-3} (Serabyn et al. 1986), and a few 10^5 cm^{-3} to a few 10^7 cm^{-3} (Jackson et al. 1993; Christopher et al. 2005; Montero-Castaño et al. 2009), respectively. The molecular gas temperature also varies, although by a much smaller factor. Measured values typically range from $\approx (50 - 200) \text{ K}$ (from HCN line ratios; Jackson et al. 1993) through $\approx (100 - 200) \text{ K}$ (from CO line ratios; Sutton et al. 1990) and up to $\approx 300 \text{ K}$ (from higher CO line ratios; Harris et al. 1985; Bradford et al. 2005). For convenience, we ignore all spatial variations (associated with either clumping or large-scale gradients) and we consider that the molecular gas has uniform density and temperature. For the temperature, an obvious choice is the intermediate value $T_{\text{m}} = 150 \text{ K}$. For the density, the assumption of uniformity means that true densities become irrelevant and that the appropriate quantity is the space-averaged density, which we derive from the ratio of the CNR mass to its volume in the next paragraph.

⁸ Remember that ϕ_{ext} is the filling factor of extended warm ionized gas within the Central Cavity, whereas ϕ_h is the filling factor of hot ionized gas inside the central 0.4 pc radius sphere alone. These filling factors must necessarily satisfy $\phi_{\text{ext}} \geq 0.91$ (value obtained if all the extended warm ionized gas is excluded from the central sphere; see next paragraph) and $\phi_h \leq 1$, respectively, thereby ruling out $\phi_h \gg \phi_{\text{ext}}$.

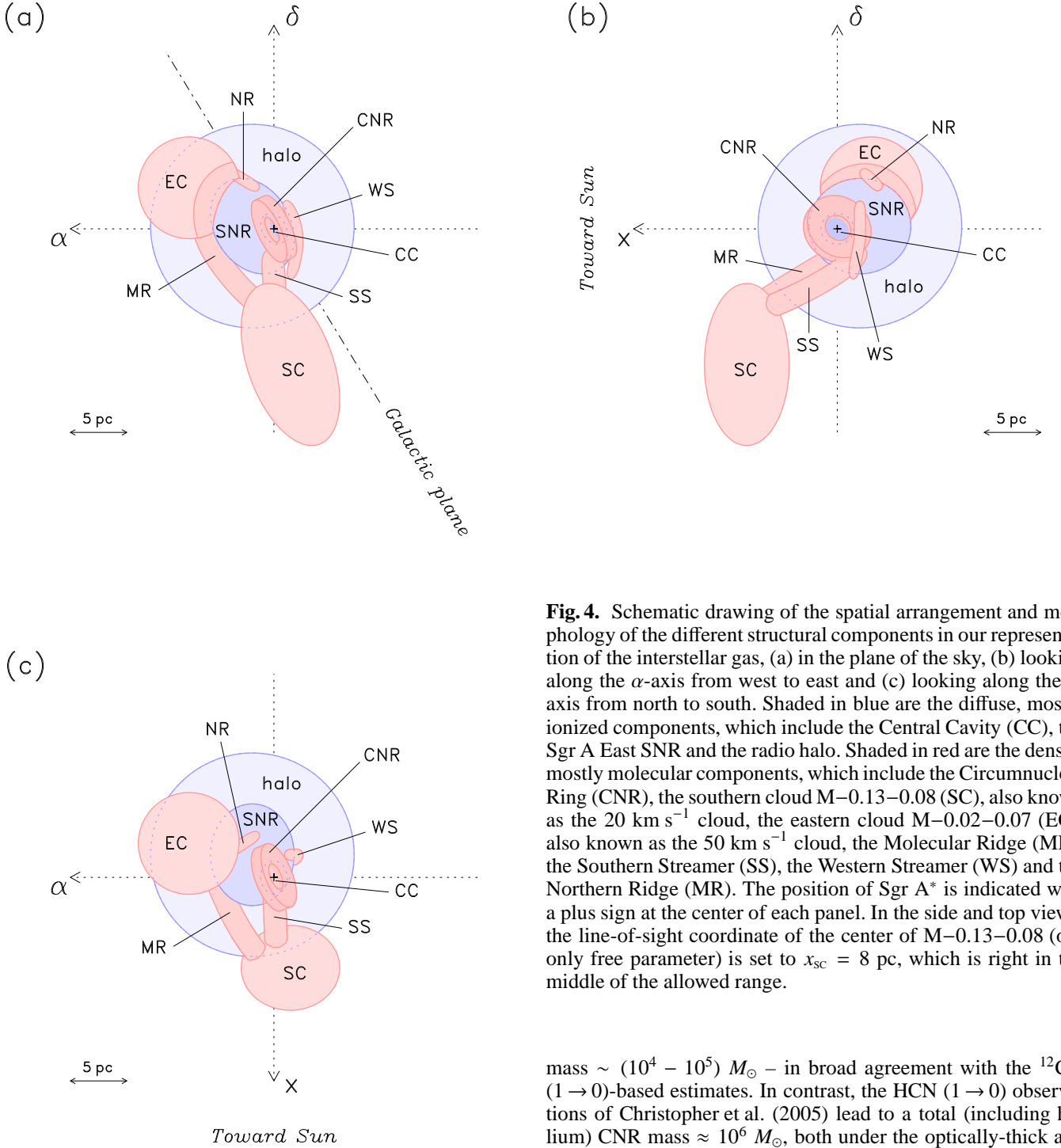


Fig. 4. Schematic drawing of the spatial arrangement and morphology of the different structural components in our representation of the interstellar gas, (a) in the plane of the sky, (b) looking along the α -axis from west to east and (c) looking along the δ -axis from north to south. Shaded in blue are the diffuse, mostly ionized components, which include the Central Cavity (CC), the Sgr A East SNR and the radio halo. Shaded in red are the denser, mostly molecular components, which include the Circumnuclear Ring (CNR), the southern cloud M–0.13–0.08 (SC), also known as the 20 km s^{−1} cloud, the eastern cloud M–0.02–0.07 (EC), also known as the 50 km s^{−1} cloud, the Molecular Ridge (MR), the Southern Streamer (SS), the Western Streamer (WS) and the Northern Ridge (NR). The position of Sgr A* is indicated with a plus sign at the center of each panel. In the side and top views, the line-of-sight coordinate of the center of M–0.13–0.08 (our only free parameter) is set to $x_{\text{sc}} = 8$ pc, which is right in the middle of the allowed range.

The molecular mass of the CNR remains extremely uncertain. ¹²CO (1 → 0) intensity measurements suggest that the CNR has an H₂ mass of a few 10⁴ M_⊙ (Genzel et al. 1985; Serabyn et al. 1986). The HCN (3 → 2) analysis of Jackson et al. (1993) yields a space-averaged H₂ density $\sim (10^4 - 10^5)$ cm^{−3}, which, multiplied by the volume $V_{\text{CNR}} = 18$ pc³, implies an H₂

mass $\sim (10^4 - 10^5)$ M_⊙ – in broad agreement with the ¹²CO (1 → 0)-based estimates. In contrast, the HCN (1 → 0) observations of Christopher et al. (2005) lead to a total (including helium) CNR mass $\approx 10^6$ M_⊙, both under the optically-thick and virial assumptions, and a similar virial mass $\approx 1.3 \times 10^6$ M_⊙ is obtained with the HCN (4 → 3) data of Montero-Castaño et al. (2009). The discrepancy between Christopher et al. (2005) (for their optically-thick mass) and Jackson et al. (1993) can obviously be attributed to the adopted HCN-to-H₂ ratios differing by a factor of 20, whereas the discrepancy between Christopher et al. (2005) (for their virial mass) and Genzel et al. (1985); Serabyn et al. (1986) can be explained if either the ¹²CO-based estimations miss a significant fraction of the mass due to gas concentration to very dense cores or if the dense HCN cores are out of virial equilibrium. In the same fashion, Oka et al. (2011) found a large discrepancy between the H₂ mass

of the CNR inferred from the measured ^{13}CO ($1 \rightarrow 0$) intensity, $\approx (2.3\text{--}5.2) \times 10^5 M_\odot$, and its virial mass, $\approx 5.7 \times 10^6 M_\odot$, which led them to reject the virial assumption. Guided by this conclusion, we choose to disregard the virial estimates, and we adopt for the H_2 mass of the CNR $(M_{\text{H}_2})_{\text{CNR}} = 2 \times 10^5 M_\odot$, as a compromise between the ^{12}CO ($1 \rightarrow 0$)- and ^{13}CO ($1 \rightarrow 0$)-based estimates. Upon dividing by $V_{\text{CNR}} = 18 \text{ pc}^3$, we then obtain for the space-averaged H_2 density in the CNR $(\langle n_{\text{H}_2} \rangle)_{\text{CNR}} = 2.2 \times 10^5 \text{ cm}^{-3}$.

The CNR also contains atomic gas, which tends to be confined to a photo-dissociated inner layer (Genzel et al. 1985; Latvakoski et al. 1999). Here, we assume that the atomic layer extends radially over 0.4 pc (Latvakoski et al. 1999), i.e., from $r_{\text{in}} = 1.2 \text{ pc}$ to $r_{\text{out,a}} = 1.6 \text{ pc}$, thereby occupying a volume of 1.65 pc^3 . We then adopt an H I mass $(M_{\text{H I}})_{\text{CNR}} = 1\,300 M_\odot$ (Latvakoski et al. 1999), so that the space-averaged H I density in the atomic layer is $(\langle n_{\text{H I}} \rangle)_{\text{CNR}} = 3.2 \times 10^4 \text{ cm}^{-3}$, intermediate between the values $\approx 1.6 \times 10^4 \text{ cm}^{-3}$ and $\approx 4.0 \times 10^4 \text{ cm}^{-3}$ derived from the measured column densities toward the southwest and northeast ends of the photo-dissociated layer (Latvakoski et al. 1999). And for the temperature of the atomic gas, we take $T_{\text{a}} = 300 \text{ K}$ (Genzel et al. 1985).

3.3. The Sgr A East SNR

In line with mainstream thought, we consider that Sgr A East is an SNR, with the observed radio synchrotron shell delimiting the swept-out cavity. To determine the relevant geometrical parameters, we rely on the 20 cm continuum map of Ekers et al. (1983), which is expected to more correctly show the full extent of the radio shell than the lower-frequency 90 cm continuum map of Pedlar et al. (1989). If we assume that, similarly to the Central Cavity, the radio shell is ellipsoidal and axisymmetric about the vertical axis, we may set its dimensions to $L_x \times L_y \times L_z = 9.0 \text{ pc} \times 9.0 \text{ pc} \times 6.7 \text{ pc}$. Accordingly, the SNR cavity has a volume $V_{\text{SNR}} = 285 \text{ pc}^3$.

Unlike the Central Cavity and the CNR, the radio shell is not centered on Sgr A*, but on a slightly offset point (x_c, y_c, z_c) . An eyeball location of the radio shell's projected center in Ekers et al.'s (1983) 20 cm map gives $y_c = 1.2 \text{ pc}$ and $z_c = -1.5 \text{ pc}$, corresponding to a projected offset of 1.9 pc, which is somewhat less than the (rescaled) value $\approx 2.1 \text{ pc}$ quoted by the authors. The determination of the line-of-sight offset, x_c , is a little more tricky. Here, we proceed from the premise (see Yusef-Zadeh et al. 2000; Maeda et al. 2002; Herrnstein & Ho 2005) that the Central Cavity lies entirely inside the radio shell and very close to its front surface. The best value (rounded to 0.1 pc) leading to this particular configuration is $x_c = -2.0 \text{ pc}$.

The SNR cavity contains hot ionized gas from both stellar ejecta and shocked interstellar matter. The former is concentrated within a central $\approx (1.7\text{--}3.2) \text{ pc}$ diameter core (Maeda et al. 2002; Sakano et al. 2004; Park et al. 2005) and has a total mass $\approx (1.4\text{--}2) M_\odot \phi_{\text{h}}^{1/2}$ (Maeda et al. 2002; Sakano et al. 2004), which represents only small fractions of the total volume and mass of hot gas inside the entire SNR cavity. This entitles us to treat all the interior hot gas as if it were of interstellar origin and to assign it a temperature $T_{\text{h}} = 1.3 \text{ keV}$ ($1.5 \times 10^7 \text{ K}$) and solar abundances, as obtained for a "plume" of shocked interstellar matter by Park et al. (2005). However, we may not take up their derived density of the "plume", which is almost certainly higher than average. Instead, we assume that the interior hot gas has a total mass of $(27 M_\odot) \phi_{\text{h}}^{1/2}$ (Koyama et al. 2007) and that it completely fills ($\phi_{\text{h}} = 1$) the volume of the SNR cavity outside the Central Cavity and the CNR, i.e., a volume of 260 pc^3 . The H^+

mass of hot gas inside the SNR cavity is then $(M_{\text{H}^+})_{\text{hot}} = 19 M_\odot$ and its (true or space-averaged) H^+ density $(n_{\text{H}^+})_{\text{h}} = 3.0 \text{ cm}^{-3}$.

3.4. The radio halo

The shape and size of the radio halo surrounding Sgr A East are fairly well established observationally. However, the fraction of the radio emission that can be attributed to thermal (warm ionized) gas is very uncertain, with some authors (e.g., Roy & Rao 2009) going so far as to question the very need for a thermal contribution. For our part, we regard the observational evidence for the presence of warm ionized gas as solid, and we assume that thermal and nonthermal gases are uniformly mixed throughout the radio halo. We model the latter as a sphere concentric with Sgr A East (see Yusef-Zadeh & Morris 1987), which approximates the 7' triangular halo of Pedlar et al. (1989) best. The result is a spherical halo centered on $(x_c, y_c, z_c) = (-2.0 \text{ pc}, 1.2 \text{ pc}, -1.5 \text{ pc})$ and having diameter $d_{\text{halo}} = 18 \text{ pc}$ and volume $V_{\text{halo}} = 3\,050 \text{ pc}^3$. The volume available to warm ionized gas within this halo is reduced by the presence of the Sgr A East SNR, the CNR and the other local molecular clouds (see Section 3.5) to $V_{\text{wi}} = 2\,440 \text{ pc}^3$. With a projected surface area of 255 pc^2 , the mean line-of-sight depth of warm ionized gas in the halo is then 9.5 pc.

For the temperature of the warm ionized gas, we choose $T_{\text{wi}} = 7\,000 \text{ K}$, which is intermediate between the temperatures used by Pedlar et al. (1989) and Anantharamaiah et al. (1999) and which is equal to the temperature adopted in Section 3.1 for the warm ionized gas inside the Central Cavity. This choice of temperature requires an up-scaling of the emission measure obtained by Pedlar et al. (1989) to $4.3 \times 10^5 \text{ pc cm}^{-6}$. With a mean line-of-sight depth of 9.5 pc and an assumed filling factor of unity, the inferred (true or space-averaged) electron density is then $(n_{\text{e}})_{\text{halo}} = 210 \text{ cm}^{-3}$. If again all the free electrons come from hydrogen, the (true or space-averaged) H^+ density in the halo is $(n_{\text{H}^+})_{\text{halo}} = (n_{\text{e}})_{\text{halo}}$ and the H^+ mass of the halo $(M_{\text{H}^+})_{\text{halo}} = 1.3 \times 10^4 M_\odot$.

Our electron density is somewhat higher than that derived by Pedlar et al. (1989), because we adopted a higher temperature and hence found a larger emission measure. However, our H^+ mass is considerably greater (by a factor ≈ 6). Obviously, the mass difference is partly due to our higher density, but the lion's share comes from our assumption that warm ionized gas fills the entire 18 pc diameter radio halo (outside Sgr A East and molecular clouds), as opposed to only its central 10 pc. The above comparison underscores the important uncertainties in the actual volume and mass of the halo gas.

3.5. The belt of molecular clouds

The nomenclature employed to distinguish different entities in the molecular belt around the Sgr A complex is not unique. The first two clouds unambiguously identified were M-0.02-0.07 to the east of Sgr A* and M-0.13-0.08 to the south (Solomon et al. 1972; Güsten et al. 1981). In NH_3 emission, M-0.02-0.07 peaks at $(l, b) \approx (-0.02^\circ, -0.07^\circ)$, corresponding to $(y, z) \approx (5.5 \text{ pc}, -3.5 \text{ pc})$, and M-0.13-0.08 peaks at $(l, b) \approx (-0.13^\circ, -0.08^\circ)$, corresponding to $(y, z) \approx (-11 \text{ pc}, -5 \text{ pc})$ (Güsten et al. 1981). In CS emission, the dense core of M-0.02-0.07 peaks at $(\Delta\alpha, \Delta\delta) \approx (3.0, 1.5)$ with respect to Sgr A*, corresponding to $(y, z) \approx (7 \text{ pc}, -4.5 \text{ pc})$ (Serabyn et al. 1992). The above transformations from (l, b) to (y, z) and from $(\Delta\alpha, \Delta\delta)$ to (y, z) were made using the $(l_{\text{A}^*}, b_{\text{A}^*}) =$

($-0^{\circ}03'20''.5$, $-0^{\circ}02'46''.3$) coordinates of Sgr A* and the $58^{\circ}60'$ angle between the (α, δ) and (y, z) systems (see Section 1).

The line-of-sight positions of both clouds are still under debate. The general belief is that M-0.13-0.08 lies in front of Sgr A* (Zylka et al. 1990; Park et al. 2004), the CNR (Coil & Ho 1999) and Sgr A East (Herrnstein & Ho 2005). Besides, M-0.13-0.08 was argued to be less than ≈ 9 pc away from Sgr A East (Coil & Ho 2000). Regarding M-0.02-0.07, a large portion of the cloud appears to lie behind Sgr A East, but there is also evidence that the cloud extends all the way to the near side of Sgr A East (Serabyn et al. 1992; Coil & Ho 2000; Herrnstein & Ho 2005; Lee et al. 2008).

Curving around the eastern edge of Sgr A East is a prominent molecular feature, usually referred to as the Molecular Ridge (or Curved Streamer). Some authors consider that the Molecular Ridge actually belongs to M-0.02-0.07 and coincides with the fraction of the cloud that has been swept up and compressed by the Sgr A East forward shock (e.g., Serabyn et al. 1992; Maeda et al. 2002). In this scenario, the Molecular Ridge must adhere to Sgr A East and form the eastern part of the gas-and-dust shell surrounding it. Other authors regard the Molecular Ridge as a separate cloud that connects M-0.02-0.07 to M-0.13-0.08, independent of Sgr A East (e.g., Herrnstein & Ho 2005; Lee et al. 2008; see also Zylka et al. 1990, who argue that the Molecular Ridge (their Curved Streamer) probably makes a true connection only with M-0.13-0.08). An intermediate possibility is that the Molecular Ridge is divided into a northern half that represents the shock-compressed portion of M-0.02-0.07 and a southern half that splits off the edge of Sgr A East and continues south toward M-0.13-0.08 (Coil & Ho 2000).

Since Sgr A East is, by all accounts, impacting upon M-0.02-0.07, a fraction of the cloud must necessarily be shock-compressed into a piece of shell, which in turn must show up as a ridge around the eastern edge of Sgr A East. It is, therefore, hard to escape the conclusion that the observed Molecular Ridge comprises shock-compressed material from M-0.02-0.07. On the other hand, the Molecular Ridge appears to extend toward M-0.13-0.08 past the boundary of M-0.02-0.07, so that it must also contain material that is *not* from M-0.02-0.07. This material could either be another piece of the shock-compressed shell surrounding Sgr A East or form a connecting bridge to M-0.13-0.08. Based on existing evidence for a physical connection between M-0.02-0.07 and M-0.13-0.08 (Lee et al. 2008), we give preference to the second possibility.

Three other elongated molecular features exist in the region of interest. Due south of Sgr A*, the Southern Streamer stretches between the CNR and M-0.13-0.08 and appears to link them together (Coil & Ho 1999). West and northeast of Sgr A*, the Western Streamer and the Northern Ridge follow (closely in the case of the Western Streamer) the contour of Sgr A East; both could be pieces of the shock-compressed shell surrounding Sgr A East (McGary et al. 2001).

The projected dimensions of the above molecular clouds have been given a range of values. Solomon et al. (1972) estimated the diameters of M-0.02-0.07 and M-0.13-0.08 at $\sim (15 - 50)$ pc. Zylka et al. (1990) found that M-0.13-0.08 is ≈ 15 pc \times 7.5 pc in size and the Molecular Ridge (their Curved Streamer) ≈ 7.5 pc wide in b . According to Coil & Ho (2000, 1999), the Molecular Ridge and the Southern Streamer are both ≈ 2 pc wide and ≥ 12 pc and ≈ 10 pc long in projection, respectively, while according to McGary et al. (2001), the Western Streamer has a north-south extent ≈ 7 pc and the Northern Ridge a northeast-southwest extent ≈ 3.5 pc. No direct information is available on the line-of-sight dimensions of these clouds.

Based on the above elements and on existing maps of the GC region, we represent the morphology and layout of the main molecular clouds in the following way:

M-0.13-0.08 is approximated as a $15 \text{ pc} \times (7.5 \text{ pc})^2$ ellipsoid (see Zylka et al. 1990), with long axis in the plane of the sky, at position angle 20° east of north, i.e., roughly parallel to the trace of the Galactic plane. Its volume is $V_{\text{SC}} = 442 \text{ pc}^3$, where subscript SC stands for southern cloud. In projection, the cloud is located south of Sgr A*, just below the southern boundary of Sgr A East, and its center, identified with the NH_3 emission peak, is at $(y_{\text{SC}}, z_{\text{SC}}) = (-11 \text{ pc}, -5 \text{ pc})$ (Güsten et al. 1981). Along the line of sight, the cloud lies completely in front of Sgr A*, within a three-dimensional distance of Sgr A East ≤ 9 pc (Coil & Ho 2000). This double constraint restricts the line-of-sight coordinate of the cloud center to the fairly loose range (in round numbers) $4 \text{ pc} \leq x_{\text{SC}} \leq 12 \text{ pc}$.

M-0.02-0.07 is most easily described starting from its original, pre-explosion shape, which we approximate as a 9 pc diameter sphere. In projection, this sphere is located at the eastern boundary of Sgr A East; its center is not identified with the NH_3 emission peak, which refers to the full present-day M-0.02-0.07 cloud (including its shock-compressed portion), but rather with the CS emission peak, which pertains to the preshock core alone and is at $(y_{\text{EC}}, z_{\text{EC}}) = (7 \text{ pc}, -4.5 \text{ pc})$ (Serabyn et al. 1992). Along the line of sight, the sphere extends from the near side to the far side of the eastern part of Sgr A East, with a small displacement toward the back; we place its center 1 pc behind the center of Sgr A East, at $x_{\text{EC}} = -3 \text{ pc}$. Here, subscript EC stands for eastern cloud.

Obviously, the fraction of the 9 pc diameter sphere that overlaps with Sgr A East has been cleared of gas by the supernova explosion, such that the swept-up gas now resides in a piece of shell squeezed between the preshock core and the Sgr A East cavity. The present-day M-0.02-0.07 cloud is thus composed of the preshock core and the piece of swept-up shell. It occupies the volume of the 9 pc diameter sphere outside Sgr A East, $V_{\text{EC}} = 356 \text{ pc}^3$, which is split between $V_{\text{EC,shell}} = 51 \text{ pc}^3$ for the piece of shell, assumed to have 1.5 times the preshock density (see below), and $V_{\text{EC,core}} = 305 \text{ pc}^3$ for the preshock core. With the above volume, the piece of shell must be 1.5 pc thick, consistent with existing maps of M-0.02-0.07.

The Molecular Ridge consists of the swept-up shell from M-0.02-0.07 and a connecting bridge to M-0.13-0.08. The "Bridge" is modeled as a curved cylinder, with diameter 2 pc (Coil & Ho 2000), extending from the southern part of M-0.02-0.07 to the northeastern end of M-0.13-0.08 along the southeastern edge of Sgr A East. The total length of the Bridge depends on the line-of-sight position of M-0.13-0.08, being between 9 pc (for $x_{\text{SC}} = 4 \text{ pc}$) and 15 pc (for $x_{\text{SC}} = 12 \text{ pc}$). Correspondingly, the volume of the Bridge is between $V_{\text{bridge}} = 28 \text{ pc}^3$ and 47 pc^3 .

The three other streamers are also modeled as curved cylinders, with diameters 2 pc for the Southern Streamer (Coil & Ho 1999) and 1 pc for the Western Streamer and the Northern Ridge (as estimated from the NH_3 maps of McGary et al. 2001).

- The Southern Streamer connects the northern end of M-0.13-0.08 to the southeastern part of the CNR. Its total length, which again depends on the line-of-sight position of M-0.13-0.08, is between 7 pc (for $x_{\text{SC}} = 4 \text{ pc}$) and 14 pc (for $x_{\text{SC}} = 12 \text{ pc}$), and its volume between $V_{\text{SS}} = 22 \text{ pc}^3$ and 44 pc^3 .
- The Western Streamer follows the western surface of Sgr A East, at the line-of-sight distance of Sgr A East's center, $x_{\text{c}} = -2 \text{ pc}$ (see footnote 6). Its total length is 8 pc and its volume $V_{\text{WS}} = 6 \text{ pc}^3$.

- The Northern Ridge extends along the northern surface of Sgr A East, in the northeast-southwest direction. Along the line-of-sight, it cannot possibly be located in front of the northeastern part of the CNR (as suggested by McGary et al. 2001); instead it lies close to (Herrnstein & Ho 2005), but behind (Lee et al. 2008) the center of Sgr A East. Its total length is 4 pc and its volume $V_{\text{NR}} = 3 \text{ pc}^3$.

We now turn to the physical conditions in the belt of molecular clouds. The gas temperature has mostly been inferred from NH_3 line ratios, leading to $\approx (50 - 120) \text{ K}$ in M–0.02–0.07 and M–0.13–0.08 (Güsten et al. 1981), $\approx (17 - 35) \text{ K}$ with a localized jump to $\approx 300 \text{ K}$ in the Southern Streamer (Coil & Ho 1999), and $\sim 15 \text{ K}$ for $\sim 75\%$ of the gas *versus* $\sim 200 \text{ K}$ for the other $\sim 25\%$ across the central 10 pc (Herrnstein & Ho 2005). Like for the other objects, we neglect the important temperature variations and adopt a uniform temperature, to which we naturally assign the mean value of Herrnstein & Ho (2005), $T_{\text{m}} = 60 \text{ K}$. This value is within the ranges derived by Güsten et al. (1981) and Coil & Ho (1999).

Little is known on either the true or space-averaged gas density in the molecular belt. From their CS observations of M–0.02–0.07, Serabyn et al. (1992) estimated the true H_2 density in the cloud at $\approx (1-2) \times 10^6 \text{ cm}^{-3}$, and with an assumed line-of-sight depth $\approx 2.5 \text{ pc}$, they obtained a space-averaged H_2 density $\approx 1.5 \times 10^4 \text{ cm}^{-3}$ in the Molecular Ridge and $\approx 3 \times 10^4 \text{ cm}^{-3}$ near the peak of the preshock core. Although a 2.5 pc line-of-sight depth is probably reasonable for the Molecular Ridge, a more appropriate choice for the peak region would be the 9 pc diameter of the preshock core, which would lower the space-averaged H_2 density to $\approx 10^4 \text{ cm}^{-3}$. For comparison, NH_3 observations of the Southern Streamer and the Molecular Ridge by Coil & Ho (1999, 2000) led to a space-averaged H_2 density $\sim (1-2) \times 10^5 \text{ cm}^{-3}$ in both streamers, assuming a line-of-sight depth $\approx 2 \text{ pc}$ and an NH_3 -to- H_2 ratio of 10^{-8} . With a presumably more realistic NH_3 -to- H_2 ratio of 10^{-7} (Herrnstein & Ho 2005), the space-averaged H_2 density would be $\sim (1-2) \times 10^4 \text{ cm}^{-3}$, in very good agreement with Serabyn et al. (1992). This good agreement prompts us to adopt $\langle n_{\text{H}_2} \rangle_{\text{streamer}} = 1.5 \times 10^4 \text{ cm}^{-3}$ in the four streamers, namely, the Molecular Ridge, the Southern Streamer, the Western Streamer and the Northern Ridge. For the preshock core of M–0.02–0.07 and for M–0.13–0.08, we rely on our downward revision of the space-averaged H_2 density near the peak of the preshock core to adopt $\langle n_{\text{H}_2} \rangle_{\text{EC,core}} = \langle n_{\text{H}_2} \rangle_{\text{sc}} = 10^4 \text{ cm}^{-3}$. It is certainly reassuring to have a space-averaged density lower in the preshock core of M–0.02–0.07 than in the Molecular Ridge (which includes the postshock portion of M–0.02–0.07).

Combining our adopted space-averaged densities with the volumes derived above, we obtain the H_2 masses listed in Table 2. Our hydrogen masses of M–0.13–0.08 and M–0.02–0.07 (either the entire cloud or its preshock core alone) are in broad agreement with existing estimates, which include $\geq 10^5 M_{\odot}$ for both clouds (from a CO emission map; Solomon et al. 1972), $\approx 3 \times 10^5 M_{\odot}$ for M–0.13–0.08 and $\geq 2 \times 10^5 M_{\odot}$ for the Sgr A East Core (from dust emission maps; Zylka et al. 1990), $\approx 1.5 \times 10^5 M_{\odot}$ for M–0.02–0.07 (from CS emission maps; Serabyn et al. 1992) and $\sim 2 \times 10^5 M_{\odot}$ for the core of M–0.02–0.07 (from NH_3 emission maps; Herrnstein & Ho 2005). Similarly, our derived hydrogen mass of the Molecular Ridge lies well within the existing range, which includes $\approx (1-1.5) \times 10^5 M_{\odot}$ (from dust emission maps; Zylka et al. 1990), $\sim 1.5 \times 10^4 M_{\odot}$ (from NH_3 emission maps, after rescaling to a NH_3 -to- H_2 ratio of 10^{-7} ; Coil & Ho 2000) and $\geq 3 \times 10^4 M_{\odot}$ (also from NH_3 emission

maps; Herrnstein & Ho 2005). In contrast, our derived hydrogen mass of the Southern Streamer is somewhat lower than the two existing NH_3 estimates, $\sim 3.5 \times 10^4 M_{\odot}$ (after rescaling to a NH_3 -to- H_2 ratio of 10^{-7} ; Coil & Ho 1999) and $\geq 8 \times 10^4 M_{\odot}$ (Herrnstein & Ho 2005). This slight discrepancy finds its origin in the very definition of the Southern Streamer. For instance, Coil & Ho (1999) considered a longer structure than we did, which extends deeper into M–0.13–0.08; what they regarded as the southern part of the Southern Streamer actually belongs to our M–0.13–0.08 cloud. Finally, for the Western Streamer and the Northern Ridge, we find hydrogen masses that are very close to the NH_3 estimates, $\sim 4 \times 10^3 M_{\odot}$ and $\sim 2 \times 10^3 M_{\odot}$, respectively (Herrnstein & Ho 2005).

4. Conclusions

Motivated by the recognized impact of the massive black hole at the dynamical center of our Galaxy and by the crucial role played by its interstellar environment, and encouraged by the multitude of recent observational findings at both long (radio and infrared) and short (X-ray and γ -ray) wavelengths, we have tried to put some order in the current muddled view of this inherently complex Galactic region. We restricted our attention to the interstellar gas within $\sim 10 \text{ pc}$ of the central black hole, and we described it in terms of five distinct structural components: the Central Cavity, the Circumnuclear Ring (CNR) encircling it, the Sgr A East SNR encompassing both, the surrounding radio halo and the belt of massive molecular clouds stretching along the Galactic plane. We first reviewed the existing observations of these five gaseous components. We then integrated them as well as possible into a detailed three-dimensional representation of the interstellar gas, in which each component is assigned both geometrical (position, shape, dimensions) and thermodynamic (phase, temperature, density, mass) characteristics. These characteristics are summarized in Tables 1 and 2, while the overall spatial disposition of the different components is graphically shown in Figure 4 from three orthogonal viewpoints.

In the process of constructing our gas representation, we inevitably came across conflicting observational claims. We naturally chose those that we found more convincing, sometimes with the benefit of hindsight, and/or those that appeared to fit the general picture better, and we disregarded the others. A synthetic list of important observational claims that we were led to push aside in favor of stronger ones is given in Table 3.

In our gas representation, the total interstellar hydrogen mass of the studied region amounts to $\approx 7 \times 10^5 M_{\odot}$. As expected, most of this mass resides in the dense, molecular components, with nearly 70% in the molecular belt and nearly 30% in the CNR. The radio halo encloses $\approx 2\%$ of the mass, the Central Cavity $\approx 0.05\%$ and the Sgr A East SNR a negligible $\approx 0.003\%$. Although the Central Cavity is commonly regarded as a spiral-shaped H II region, only half its mass is actually in the form of warm ionized gas, and barely $\approx 3\%$ is truly contained in the Minispiral; the other half of the mass belongs to neutral atomic streamers.

Our gas representation is merely meant to provide a three-dimensional snapshot of the innermost interstellar region as it presently stands, not to explain how this highly interacting system actually works. However, to set the general framework, we were led to briefly discuss the physical interactions between the different gaseous components. This also helped us to constrain their positional relationships (primarily along the line of sight), in the light of the available observational data on their morphology, kinematics, absorption-versus-emission properties, etc.

Table 3. Observational claims disregarded in our gas representation.

	Claims	References
Central Cavity	The diffuse cm radio continuum emission from Sgr A West is mainly nonthermal.	Ekers et al. (1983)
	The Western Arc and the Northern Arm are contained in a single one-armed linear spiral.	Lo & Claussen (1983)
	Ionized gas in the Northern Arm is on an unbound orbit about Sgr A*.	Roberts et al. (1996)
		Yusef-Zadeh et al. (1998)
CNR	The Northern and Eastern Arms are the ionized outer rims of the Northern Streamer.	Mužić et al. (2007)
		Davidson et al. (1992)
	The CNR is off-centered from Sgr A* and noticeably warped.	Jackson et al. (1993)
		Güsten et al. (1987)
Sgr A East	Dense molecular cores inside the CNR are in virial equilibrium.	Christopher et al. (2005)
		Montero-Castaño et al. (2009)
	Sgr A East is separated from Sgr A West by a finite distance along the line of sight.	Karlsson et al. (2003)
		Sjouwerman & Pihlström (2008)
Radio halo	The radio halo is purely nonthermal.	Roy & Rao (2009)
	The radio halo is located in front of Sgr A East.	Pedlar et al. (1989)
Molecular belt	The Curved Streamer (or Molecular Ridge) is a northward extension of M–0.13–0.08, separate from M–0.02–0.07.	Zylka et al. (1990)
	The Molecular Ridge as a whole is the shock-compressed portion of M–0.02–0.07.	Serabyn et al. (1992)
		Maeda et al. (2002)
	The Molecular Ridge is a separate cloud connecting M–0.02–0.07 to M–0.13–0.08.	Herrnstein & Ho (2005)
		Lee et al. (2008)
	The Northern Ridge sits in front of the northeastern lobe of the CNR.	McGary et al. (2001)
	The Western Streamer is highly inclined to the plane of the sky.	Herrnstein & Ho (2005)
	The 20 km s ^{−1} cloud lies mostly behind Sgr A West.	Karlsson et al. (2003)
		Sjouwerman & Pihlström (2008)

As we learned along the way, much of the present state of the innermost interstellar region is likely the direct result of two antagonistic phenomena, namely, unsteady accretion onto the central black hole and rapid expansion triggered by a nearby supernova explosion. The CNR is almost certainly a manifestation of the accretion, and so are also several of the local streamers, including the ionized Northern and Eastern Arms of the Minispiral, their neutral counterparts in the Central Cavity and, in a less obvious manner, the Southern Streamer, which was found to carry material from the M–0.13–0.08 GMC to the CNR. Meanwhile, the supernova explosion may be held responsible for the existence of Sgr A East and of most of the dense and elongated features observed along its projected boundary – the gas-and-dust shell, all or part of the Molecular Ridge, the Western Streamer and probably the Northern Ridge. Interestingly, the CNR itself might be a by-product of the explosion, formed as the gas-and-dust shell swept up by the supernova shock passed over Sgr A* and left a piece in its deep gravitational potential. In this case, the CNR would offer a nice illustration of the complex interplay between supernova-driven expansion and black-hole accretion.

A self-consistent and reliable three-dimensional snapshot of the innermost interstellar gas, which incorporates all relevant information from diverse observational sources, may serve several purposes. First and foremost, such a snapshot may constitute an objective reference against which to test different scenarios of the intricate dynamics of the region as well as of the detailed operation of the whole nuclear engine, with the precise role played by each of its (stellar and interstellar) constituents. This, in turn, may pave the way to improve our understanding of galactic nuclei in general. In a different perspective, our gas representation may provide the necessary framework to study specific prob-

lems related to Sgr A* and its immediate environment. As mentioned in the introduction, the problem that we personally have in mind bears on the propagation and annihilation of positrons from Sgr A*.

In its present form, our gas representation still suffers from many uncertainties. Perhaps most uncertain of all is the line-of-sight location of the M–0.13–0.08 GMC, which we left as a free parameter (albeit restricted to a narrowed-down range). Another uncertain aspect concerns the true nature of what we referred to as the Molecular Ridge – whether all of it represents a piece of the shock-compressed shell surrounding Sgr A East or whether its southern half forms a separate bridge between M–0.02–0.07 and M–0.13–0.08. Equally uncertain are the number of neutral streamers inside the Central Cavity and their exact relationship with the ionized Northern and Eastern Arms of the Minispiral. And of course, none of the thermodynamic parameters is really well constrained. Hopefully, future observations will help to sort out the remaining uncertainties.

Acknowledgements. The author expresses her gratitude to N. Guessoum, P. Jean, J. Knödlseider, S. Park and F. Yusef-Zadeh for enlightening discussions and help with the preparation of the manuscript.

References

- Aitken, D. K., Smith, C. H., Moore, T. J. T., & Roche, P. F. 1998, MNRAS, 299, 743
- Amo-Baladrón, M. A., Martín-Pintado, J., & Martín, S. 2011, A&A, 526, A54+
- Amo-Baladrón, M. A., Martín-Pintado, J., Morris, M. R., Muno, M. P., & Rodríguez-Fernández, N. J. 2009, ApJ, 694, 943
- Anantharamaiah, K. R., Pedlar, A., & Goss, W. M. 1999, in Astronomical Society of the Pacific Conference Series, Vol. 186, The Central Parsecs of

- the Galaxy, ed. H. Falcke, A. Cotera, W. J. Duschl, F. Melia, & M. J. Rieke, 422–+
- Baganoff, F. K., Maeda, Y., Morris, M., et al. 2003, *ApJ*, 591, 891
- Beckert, T., Duschl, W. J., Mezger, P. G., & Zylka, R. 1996, *A&A*, 307, 450
- Becklin, E. E., Gatley, I., & Werner, M. W. 1982, *ApJ*, 258, 135
- Blum, R. D., Ramírez, S. V., Sellgren, K., & Olsen, K. 2003, *ApJ*, 597, 323
- Bradford, C. M., Stacey, G. J., Nikola, T., et al. 2005, *ApJ*, 623, 866
- Brown, R. L. & Liszt, H. S. 1984, *ARA&A*, 22, 223
- Burton, M. & Allen, D. 1992, *Proceedings of the Astronomical Society of Australia*, 10, 55
- Christopher, M. H., Scoville, N. Z., Stolovy, S. R., & Yun, M. S. 2005, *ApJ*, 622, 346
- Coil, A. L. & Ho, P. T. P. 1999, *ApJ*, 513, 752
- Coil, A. L. & Ho, P. T. P. 2000, *ApJ*, 533, 245
- Davidson, J. A., Werner, M. W., Wu, X., et al. 1992, *ApJ*, 387, 189
- Dent, W. R. F., Matthews, H. E., Wade, R., & Duncan, W. D. 1993, *ApJ*, 410, 650
- Depoy, D. L., Gatley, I., & McLean, I. S. 1989, in *IAU Symposium*, Vol. 136, *The Center of the Galaxy*, ed. M. Morris, 411–+
- Ekers, R. D., Goss, W. M., Schwarz, U. J., Downes, D., & Rogstad, D. H. 1975, *A&A*, 43, 159
- Ekers, R. D., van Gorkom, J. H., Schwarz, U. J., & Goss, W. M. 1983, *A&A*, 122, 143
- Gatley, I., Beattie, D. H., Lee, T. J., Jones, T. J., & Hyland, A. R. 1984, *MNRAS*, 210, 565
- Gatley, I., Jones, T. J., Hyland, A. R., et al. 1986, *MNRAS*, 222, 299
- Geballe, T. R., Krisciunas, K., Bailey, J. A., & Wade, R. 1991, *ApJ*, 370, L73
- Genzel, R., Crawford, M. K., Townes, C. H., & Watson, D. M. 1985, *ApJ*, 297, 766
- Genzel, R., Eisenhauer, F., & Gillessen, S. 2010, *Reviews of Modern Physics*, 82, 3121
- Güsten, R. & Downes, D. 1980, *A&A*, 87, 6
- Güsten, R., Genzel, R., Wright, M. C. H., et al. 1987, *ApJ*, 318, 124
- Güsten, R., Walmsley, C. M., & Pauls, T. 1981, *A&A*, 103, 197
- Hall, D. N. B., Kleinmann, S. G., & Scoville, N. Z. 1982, *ApJ*, 260, L53
- Harris, A. I., Jaffe, D. T., Silber, M., & Genzel, R. 1985, *ApJ*, 294, L93
- Herbst, T. M., Beckwith, S. V. W., Forrest, W. J., & Pipher, J. L. 1993, *AJ*, 105, 956
- Herrnstein, R. M. & Ho, P. T. P. 2002, *ApJ*, 579, L83
- Herrnstein, R. M. & Ho, P. T. P. 2005, *ApJ*, 620, 287
- Jackson, J. M., Geis, N., Genzel, R., et al. 1993, *ApJ*, 402, 173
- Jones, T. W. 1974, *A&A*, 30, 37
- Karlsson, R., Sjouwerman, L. O., Sandqvist, A., & Whiteoak, J. B. 2003, *A&A*, 403, 1011
- Koyama, K., Uchiyama, H., Hyodo, Y., et al. 2007, *PASJ*, 59, 237
- Krabbe, A., Genzel, R., Drapatz, S., & Rotaciuc, V. 1991, *ApJ*, 382, L19
- Krabbe, A., Genzel, R., Eckart, A., et al. 1995, *ApJ*, 447, L95+
- Lacy, J. H., Achtermann, J. M., & Serabyn, E. 1991, *ApJ*, 380, L71
- Lacy, J. H., Baas, F., Townes, C. H., & Geballe, T. R. 1979, *ApJ*, 227, L17
- Lacy, J. H., Townes, C. H., Geballe, T. R., & Hollenbach, D. J. 1980, *ApJ*, 241, 132
- Latvakoski, H. M., Stacey, G. J., Gull, G. E., & Hayward, T. L. 1999, *ApJ*, 511, 761
- Lee, S., Pak, S., Choi, M., et al. 2008, *ApJ*, 674, 247
- Lee, S., Pak, S., Davis, C. J., et al. 2003, *MNRAS*, 341, 509
- Lis, D. C. & Carlstrom, J. E. 1994, *ApJ*, 424, 189
- Liszt, H. S. 2003, *A&A*, 408, 1009
- Liszt, H. S., Burton, W. B., & van der Hulst, J. M. 1985, *A&A*, 142, 237
- Liszt, H. S., van der Hulst, J. M., Burton, W. B., & Ondrechen, M. P. 1983, *A&A*, 126, 341
- Lo, K. Y. & Claussen, M. J. 1983, *Nature*, 306, 647
- Lutz, D., Krabbe, A., & Genzel, R. 1993, *ApJ*, 418, 244
- Maeda, Y., Baganoff, F. K., Feigelson, E. D., et al. 2002, *ApJ*, 570, 671
- Marr, J. M., Wright, M. C. H., & Backer, D. C. 1993, *ApJ*, 411, 667
- Marshall, J., Lasenby, A. N., & Harris, A. I. 1995, *MNRAS*, 277, 594
- McGary, R. S., Coil, A. L., & Ho, P. T. P. 2001, *ApJ*, 559, 326
- Melia, F., Coker, R. F., & Yusef-Zadeh, F. 1996, *ApJ*, 460, L33+
- Mezger, P. G., Duschl, W. J., & Zylka, R. 1996, *A&A Rev.*, 7, 289
- Mezger, P. G., Zylka, R., Salter, C. J., et al. 1989, *A&A*, 209, 337
- Montero-Castaño, M., Herrnstein, R. M., & Ho, P. T. P. 2009, *ApJ*, 695, 1477
- Morris, M. & Serabyn, E. 1996, *ARA&A*, 34, 645
- Morris, M. & Yusef-Zadeh, F. 1987, in *American Institute of Physics Conference Series*, Vol. 155, *The Galactic Center*, ed. D. C. Backer, 127–132
- Mužić, K., Eckart, A., Schödel, R., Meyer, L., & Zensus, A. 2007, *A&A*, 469, 993
- Oka, T., Nagai, M., Kamegai, K., & Tanaka, K. 2011, *ApJ*, 732, 120
- Okumura, S. K., Ishiguro, M., Fomalont, E. B., et al. 1989, *ApJ*, 347, 240
- Okumura, S. K., Ishiguro, M., Fomalont, E. B., et al. 1991, *ApJ*, 378, 127
- Park, S., Muno, M. P., Baganoff, F. K., et al. 2005, *ApJ*, 631, 964
- Park, S., Muno, M. P., Baganoff, F. K., et al. 2004, *ApJ*, 603, 548
- Paumard, T., Genzel, R., Martins, F., et al. 2006, *ApJ*, 643, 1011
- Paumard, T., Maillard, J.-P., & Morris, M. 2004, *A&A*, 426, 81
- Pedlar, A., Anantharamaiah, K. R., Ekers, R. D., et al. 1989, *ApJ*, 342, 769
- Poglitsch, A., Stacey, G. J., Geis, N., et al. 1991, *ApJ*, 374, L33
- Reid, M. J. & Brunthaler, A. 2004, *ApJ*, 616, 872
- Roberts, D. A. & Goss, W. M. 1993, *ApJS*, 86, 133
- Roberts, D. A., Yusef-Zadeh, F., & Goss, W. M. 1996, *ApJ*, 459, 627
- Rockefeller, G., Fryer, C. L., Melia, F., & Warren, M. S. 2004, *ApJ*, 604, 662
- Roy, S. & Rao, A. P. 2009, in *Astronomical Society of the Pacific Conference Series*, Vol. 407, *The Low-Frequency Radio Universe*, ed. D. J. Saikia, D. A. Green, Y. Gupta, & T. Venturi, 267–+
- Sakano, M., Warwick, R. S., Decourchelle, A., & Predehl, P. 2004, *MNRAS*, 350, 129
- Sanders, R. H. 1998, *MNRAS*, 294, 35
- Sandqvist, A. 1974, *A&A*, 33, 413
- Sandqvist, A., Larsson, B., Hjalmarson, Å., et al. 2008, *A&A*, 482, 849
- Schödel, R., Eckart, A., Alexander, T., et al. 2007, *A&A*, 469, 125
- Schödel, R., Merritt, D., & Eckart, A. 2009, *A&A*, 502, 91
- Schwarz, U. J., Bregman, J. D., & van Gorkom, J. H. 1989, *A&A*, 215, 33
- Serabyn, E., Güsten, R., & Evans, II, N. J. 1989, in *IAU Symposium*, Vol. 136, *The Center of the Galaxy*, ed. M. Morris, 417–+
- Serabyn, E., Güsten, R., Walmsley, J. E., Wink, J. E., & Zylka, R. 1986, *A&A*, 169, 85
- Serabyn, E. & Lacy, J. H. 1985, *ApJ*, 293, 445
- Serabyn, E., Lacy, J. H., & Achtermann, J. M. 1992, *ApJ*, 395, 166
- Serabyn, E., Lacy, J. H., Townes, C. H., & Bharat, R. 1988, *ApJ*, 326, 171
- Shukla, H., Yun, M. S., & Scoville, N. Z. 2004, *ApJ*, 616, 231
- Sjouwerman, L. O. & Pihlström, Y. M. 2008, *ApJ*, 681, 1287
- Solomon, P. M., Scoville, N. Z., Penzias, A. A., Wilson, R. W., & Jefferts, K. B. 1972, *ApJ*, 178, 125
- Stankovic, M., Seaquist, E. R., Mühle, S., Leurini, S., & Menten, K. M. 2007, in *Molecules in Space and Laboratory*
- Sutton, E. C., Danchi, W. C., Jaminet, P. A., & Masson, C. R. 1990, *ApJ*, 348, 503
- Telesco, C. M., Davidson, J. A., & Werner, M. W. 1996, *ApJ*, 456, 541
- Tripp, S., Gillessen, S., Gerhard, O. E., et al. 2008, *A&A*, 492, 419
- Tsuboi, M., Handa, T., & Ukita, N. 1999, *ApJS*, 120, 1
- Tsuboi, M., Miyazaki, A., & Okumura, S. K. 2009, *PASJ*, 61, 29
- Tsuboi, M., Okumura, S. K., & Miyazaki, A. 2006, *Journal of Physics Conference Series*, 54, 16
- van Gorkom, J. H., Schwarz, U. J., & Bregman, J. D. 1985, in *IAU Symposium*, Vol. 106, *The Milky Way Galaxy*, ed. H. van Woerden, R. J. Allen, & W. B. Burton, 371–376
- Viehmann, T., Eckart, A., Schödel, R., et al. 2005, *A&A*, 433, 117
- Vollmer, B. & Duschl, W. J. 2000, *New A*, 4, 581
- Wardle, M. & Yusef-Zadeh, F. 1992, *Nature*, 357, 308
- Whiteoak, J. B., Rogstad, D. H., & Lockhart, I. A. 1974, *A&A*, 36, 245
- Wright, G. S., McLean, I. S., & Bland, J. 1989, in *ESA Special Publication*, Vol. 290, *Infrared Spectroscopy in Astronomy*, ed. E. Böhm-Vitense, 425–428
- Wright, M. C. H., Coil, A. L., McGary, R. S., Ho, P. T. P., & Harris, A. I. 2001, *ApJ*, 551, 254
- Yuan, F. 2006, *Journal of Physics Conference Series*, 54, 427
- Yusef-Zadeh, F., Braatz, J., Wardle, M., & Roberts, D. 2008, *ApJ*, 683, L147
- Yusef-Zadeh, F. & Melia, F. 1992, *ApJ*, 385, L41
- Yusef-Zadeh, F., Melia, F., & Wardle, M. 2000, *Science*, 287, 85
- Yusef-Zadeh, F. & Morris, M. 1987, *ApJ*, 320, 545
- Yusef-Zadeh, F. & Morris, M. 1991, *ApJ*, 371, L59
- Yusef-Zadeh, F., Morris, M., & Ekers, R. 1989, in *IAU Symposium*, Vol. 136, *The Center of the Galaxy*, ed. M. Morris, 443–+
- Yusef-Zadeh, F., Roberts, D. A., & Biretta, J. 1998, *ApJ*, 499, L159+
- Yusef-Zadeh, F., Roberts, D. A., Goss, W. M., Frail, D. A., & Green, A. J. 1996, *ApJ*, 466, L25+
- Yusef-Zadeh, F., Roberts, D. A., Goss, W. M., Frail, D. A., & Green, A. J. 1999a, *ApJ*, 512, 230
- Yusef-Zadeh, F., Stolovy, S. R., Burton, M., Wardle, M., & Ashley, M. C. B. 2001, *ApJ*, 560, 749
- Yusef-Zadeh, F., Stolovy, S. R., Burton, M., et al. 1999b, in *Astronomical Society of the Pacific Conference Series*, Vol. 186, *The Central Parsecs of the Galaxy*, ed. H. Falcke, A. Cotera, W. J. Duschl, F. Melia, & M. J. Rieke, 197–+
- Yusef-Zadeh, F. & Wardle, M. 1993, *ApJ*, 405, 584
- Zhao, J., Morris, M. R., Goss, W. M., & An, T. 2009, *ApJ*, 699, 186
- Zhao, J.-H., Blundell, R., Moran, J. M., et al. 2010, *ApJ*, 723, 1097
- Zylka, R., Mezger, P. G., Ward-Thompson, D., Duschl, W. J., & Lesch, H. 1995, *A&A*, 297, 83
- Zylka, R., Mezger, P. G., & Wink, J. E. 1990, *A&A*, 234, 133